



HAL
open science

Asymmetric reverse transition phenomenon in internal turbulent channel flows due to temperature gradients

Sylvain Serra, Erwin Franquet, Valentin Boutrouche, Remi Manceau

► To cite this version:

Sylvain Serra, Erwin Franquet, Valentin Boutrouche, Remi Manceau. Asymmetric reverse transition phenomenon in internal turbulent channel flows due to temperature gradients. *International Journal of Thermal Sciences*, 2021, 159 (106463), 10.1016/j.ijthermalsci.2020.106463 . hal-02923557

HAL Id: hal-02923557

<https://hal.science/hal-02923557>

Submitted on 27 Aug 2020

HAL is a multi-disciplinary open access archive for the deposit and dissemination of scientific research documents, whether they are published or not. The documents may come from teaching and research institutions in France or abroad, or from public or private research centers.

L'archive ouverte pluridisciplinaire **HAL**, est destinée au dépôt et à la diffusion de documents scientifiques de niveau recherche, publiés ou non, émanant des établissements d'enseignement et de recherche français ou étrangers, des laboratoires publics ou privés.



Distributed under a Creative Commons Attribution - NonCommercial - NoDerivatives 4.0 International License

Asymmetric reverse transition phenomenon in internal turbulent channel flows due to temperature gradients

Sylvain Serra[†], Erwin Franquet^{†,*}, Valentin Boutrouche*, Rémi Manceau[‡]

[†] Université de Pau et des Pays de l'Adour, E2S UPPA, LaTEP, Pau, France,

* Department of Mechanical Engineering, University of Massachusetts Lowell, One University Avenue, Lowell, MA 01854, USA

[‡] CNRS, Université de Pau et des Pays de l'Adour, E2S UPPA, INRIA, équipe CAGIRE, LMAP, Pau, France

* corresponding author (erwin.franquet@univ-pau.fr)

Laminarization of a turbulent flow due to wall heating has been known for more than 50 years, to the point that it is sometimes used as means of reducing friction. However this phenomenon has been mainly studied for cylindrical pipes and with imposed heat flux but not for channel flows and with imposed temperature boundary conditions, especially with asymmetric ones (that is to say in presence of a transverse thermal gradient). Based on the recent success of some Reynolds-averaged Navier-Stokes (RANS) models to correctly describe the influence of a strong transverse temperature gradient on turbulent Poiseuille flows, when compared to similar direct numerical simulations (DNS) or large eddy simulations (LES) results, these approaches are used here to investigate reverse transition. Since the choice of turbulence model has a non-negligible influence on the results, however, it is necessary to use different models to get an indication of the uncertainty associated with them. The proposed methodology is based on the use of RANS closures that do not involve any wall functions due to the strong gradient in the wall layer that has to be modeled. Thus, two first-moment closures and a second-moment closure are considered: the $k - \omega - SST$ and the $k - \varepsilon - \overline{v^2}/k$, and the EB-RSM. The latter two rely on an elliptic blending. The turbulent heat flux is modeled with a simple gradient diffusion hypothesis (SGDH) and a generalized gradient diffusion hypothesis (GGDH) for the first-moment and second-moment closures respectively. In summary, more than 800 calculations are performed for the above three models in order to analyze the reverse transition, and to open room for debate on the possibility for such approaches to correctly reproduce the experimentally observed behavior.

Keywords: turbulent channel flow, transverse temperature gradient, flow asymmetry, relaminarization, elliptic blending

Contents

Nomenclature	3
1 Introduction	4
1.1 Foreword	4
1.2 Literature review	4
1.3 Novelty of the study	5
2 Problem statement	7
2.1 Description	7
2.2 Modeling	11
3 Results	12
4 Conclusion	33
References	39
A Overview of some available studies dealing with thermal effects on turbulent flows	40
B RANS models	42
B.1 $k - \omega - SST$ equations	42
B.2 $k - \varepsilon - v^2/k$ equations	42
B.3 EB-RSM equations	43

Nomenclature

Latin symbols

c_P	specific heat capacity, $\text{J kg}^{-1} \text{K}^{-1}$
h	height, m
k	turbulent kinetic energy, $\text{m}^2 \text{s}^{-2}$
L	length, m
P	pressure, Pa
Pr	Prandtl number, –
R	individual ideal gas constant, $\text{J kg}^{-1} \text{K}^{-1}$
Re	Reynolds number, –
S_{ij}	strain tensor, s^{-1}
T	temperature, K
t	time, s
U_i	i^{th} component of the velocity vector, m s^{-1}
x_i	i^{th} component of the position vector, m
y	distance to the wall, m
y^+	distance to the wall in wall units, –

Greek symbols

δ_{ij}	Kronecker symbol, –
β	momentum source term, Pa m^{-1}
ε	turbulent dissipation rate, $\text{m}^2 \text{s}^{-3}$
λ	thermal conductivity, $\text{W K}^{-1} \text{m}^{-1}$
μ	dynamic viscosity, $\text{kg m}^{-1} \text{s}^{-1}$
ν	kinematic viscosity, $\text{m}^2 \text{s}^{-1}$
ρ	density, kg m^{-3}
τ	viscous tensor, Pa
ω	specific dissipation rate, s^{-1}

Subscripts and superscripts

*	critical value
1	cold wall
2	hot wall
\overline{X}	Favre average of the variable X
X'	fluctuation of the variable X
b	bulk
h	homogeneous
M	mean
m	mean (average)
r	ratio
t	turbulent
w	wall
τ	friction

Acronyms

DNS	direct numerical simulation
EB	elliptic blending
GGDH	generalized gradient diffusion hypothesis
LES	large eddy simulation
RANS	Reynolds-averaged Navier–Stokes
RSM	Reynolds-stress model
SGDH	simple gradient diffusion hypothesis
SSG	Speziale–Sarkar–Gatski
SST	shear stress transport

1 Introduction

1.1 Foreword

Reverse transition, also known as laminarization or reversion, concerns the evolution of an initially turbulent flow towards a laminar one yet still with fluctuations, under the effect of re-acceleration, curvature, rotation or heat transfer [1]. Generally speaking, this transition should not be understood as a spatial one but rather as a local modification and a behavioral change in the flow variables.

From an industrial point of view, this phenomenon is of particular importance since it can lead to a strong decrease of the heat transfer and then to possible damage of the devices. The latter case is the one pertaining to the present study. In such a case, the occurrence of laminarization was reviewed by [2] for pipes and by [3] for vertical pipes undergoing mixed convection, while [4] focused on the impact on the heat transfer coefficients and [5] extended this work to non-circular ducts.

1.2 Literature review

Firstly, a brief summary of the available studies dealing with reversion is given in Table 1. It is straightforward to notice that most of the studies focus on imposed heat flux [6–25] whereas Dirichlet boundary conditions types are very scant [26,27]. Cylindrical pipes are the most frequently encountered geometry [7,9,12,14,16,18,20,23,25] while channels are scarcer [6,8,13,17,26,27]. This scarcity obviously creates an impetus for the analysis of laminarization in turbulent channel flows with imposed temperature at the walls. At the same time, such a situation has been the topic of many papers, mainly based on DNS or LES approaches; these papers are reviewed in [28] and summarized in a table reproduced below as Table 2. Lastly, re-laminarization is only mentioned in [29,32].

In these two sets of papers, it appears that temperature is very often considered as a passive scalar and/or not related to the thermophysical properties, be it for DNS [26,27,33–43] or for RANS studies [9,11,13,15]. In contrast, the influence of temperature on the property variations is still underdeveloped in DNS [44,48] and LES [29,32,49–51] and RANS papers [14,17,24,25,52]. Furthermore, the vast majority of these studies only consider fully developed features; for instance, the few available DNS databases are built within this framework. To the best of the authors' knowledge, the analysis of the laminarization phenomenon for turbulent channel flows with Dirichlet boundary conditions has not been performed with RANS calculations up to now. More importantly, the few RANS papers with imposed heat-flux have shown that no sufficient accuracy was obtained [11,52] even with a modified closure considering also a two-equation modeling for the thermal field [53].

Nevertheless, it has been shown recently that, in certain circumstances, RANS calculations can predict relatively well the overall behavior of internal turbulent channel flows with transverse temperature gradients due to asymmetric thermal boundary conditions [28]. Comparisons with available DNS or LES results show that non-dimensional mean velocities and temperatures are correctly described, especially the asymmetry observed in such situations. It was also demonstrated, however, that this is not always straightforward, since thermal closure is a major cornerstone of RANS modeling: the commonly implemented SGDH clearly failed when used with second-moment closure. Moreover, it has been shown [28] that, although the different models are capable of reproducing the essential physical phenomena observed, their results show significant discrepancies. Therefore, quantitative conclusions should be drawn with great care, and in particular, it is recommended that the results of different models be compared to get an idea of the uncertainty associated with modelling. Meanwhile, it has been clearly highlighted that the temperature dependency of the physical properties yields a strong differentiation of the dynamic and thermal fields on both sides, *i.e.* close to the cold and hot walls, with corresponding friction Reynolds numbers approaching the re-laminarization zone. Last but not least, available known DNS or LES results are very scant for high temperature ratios. The onus of the real fluid behavior under such circumstances thus still remains to be shown.

1.3 Novelty of the study

The goal of the present study is to further investigate reverse transition for horizontal forced flows in differentially isothermally heated channels, that is to say in channels with Dirichlet boundary conditions where the imposed temperatures are different on the opposite sides. The low-Mach number approximation is considered, together with temperature-dependent properties, the density being modeled by the standard perfect gas law and the molecular viscosity and thermal conductivity by Sutherland's law [54]. This work is performed with the help of RANS calculations, since the hundreds of calculations to be performed are unreachable with DNS or even LES. For example, the recent study of Flageul *et al.* using DNS and LES [55], in a similar configuration but with a different objective, shows that a very limited number of parameters can be studied with such expensive methodologies. Thus, RANS remains the only option to span sufficient parameter space. Added to this, even wall-refined LES would not be reliable enough, since the prediction of relaminarization is dependent on the subgrid scale mode [56]. More specifically, the involved models propose near-wall turbulence modeling: the $k - \omega - SST$ of Menter [57, 58], and the $k - \varepsilon - \overline{v^2}/k$ elliptic eddy-viscosity model of Billard and Laurence [59]; and the elliptic-blending Reynolds-stress model (EB-RSM) of Manceau *et al.* [60, 61]. The turbulent heat flux was computed using the SGDH and the GGDH approach for the first-moment and second-moment closures respectively. As mentioned above, these three models reproduce the essential phenomena observed in the reference databases [28], but give quantitatively different results. Performing the parametric study with these three models will allow us to have an order of magnitude of uncertainty related to the modeling choices.

The aim of the present paper is thus to propose an exploratory study on the capabilities of RANS calculations to retrieve laminarization due to thermal effects and to predict its onset for a large screening of various physical parameters, namely the friction Reynolds number and the temperature ratio between the cold and hot wall. Due to the favorable speed of such calculations, a great number of operating conditions were investigated; concretely, it corresponds to 17 temperature ratios and 16 turbulent Reynolds numbers for the 3 RANS closures, which means $17 \times 16 \times 3 = 816$ cases. In comparison, it would have been impossible with DNS or LES to perform such calculations for the range of parameters spanned in the present paper.

The paper is organized as follows: section [2] is devoted to the presentation of the problem and its modeling, while section [3] presents the results. Finally, conclusions are drawn in section [4]

Table 1 – Studies on reverse transition due to thermal effects

Ref.	Type	Flow			Geometry				Orient.		Thermal cond.			Modelling	
		forced	natural	mixed	plate	tube	annulus	channel	hor.	ver.	imp. temp.	imp. flux	heat source	passive scal.	dep. param.
C.A. Bankston, 1970 [6]	Exp.	✓				✓				✓					n.a.
C.W. Coon and K.W. Perkins, 1970 [7]	Exp.	✓				✓				✓					n.a.
K.R. Perkins <i>et al.</i> , 1973 [8]	Exp.	✓		✓				✓		✓					n.a.
S. Torii <i>et al.</i> , 1990 [9]	RANS	✓				✓								✓	
S. Torii <i>et al.</i> , 1991 [10]	RANS	✓					✓		✓					✓	
S. Torii and W.-J. Yang, 1997 [11]	RANS	✓				✓			✓					✓	
A.M. Shehata and D.M. McEligot, 1998 [12]	Exp.	✓				✓				✓					n.a.
S. Torii and W.-J. Yang, 2000 [13]	RANS	✓						✓	✓					✓	
D.P. Mikielewicz <i>et al.</i> , 2002 [14]	RANS	✓				✓				✓					✓
S. Torii and W.-J. Yang, 2005 [15]	RANS	✓				✓			✓					✓	
J.H. Bae <i>et al.</i> , 2005 [16]	DNS	✓		✓		✓				✓					✓
S. Gordev <i>et al.</i> , 2005 [17]	RANS	✓						✓	✓						✓
J.H. Bae <i>et al.</i> , 2006 [18]	DNS	✓		✓		✓				✓					✓
J.H. Bae <i>et al.</i> , 2008 [19]	DNS	✓		✓			✓			✓				✓	✓
S. He <i>et al.</i> , 2008 [20]	DNS	✓		✓		✓				✓					✓
S. He <i>et al.</i> , 2008 [21]	RANS	✓		✓		✓				✓					✓
J.I. Lee <i>et al.</i> , 2008 [22]	Exp.			✓		✓				✓					n.a.
J.I. Lee <i>et al.</i> , 2008 [23]	Exp.			✓		✓				✓					n.a.
Y. chen <i>et al.</i> , 2012 [24]	RANS	✓						✓	✓						✓
F. Zonta <i>et al.</i> , 2012 [26]	DNS	✓						✓	✓			✓		✓	
F. Zonta <i>et al.</i> , 2012 [27]	DNS			✓				✓	✓			✓		✓	
B. Shome, 2014 [25]	RANS	✓		✓		✓		✓	✓			✓			✓
A. Pucciarelli and W. Ambrosini, 2017 [52]	RANS		✓					✓	✓			✓		✓	

Table 2 – Studies on non-isothermal turbulent flows with asymmetric wall temperatures

T_r		1	1.01	1.02	1.07	2	3	5	6	8	9
180	DNS	[37][62]	[44][45]			[44][46]					
	LES	[32][63][64]	[31][32][51][63][65]	[29]		[31][32][51][64]	[29][51]	[32][51]	[31]	[31]	[31]
395	DNS	[37][46][62]				[46]					
	LES	[32][64]	[51]		[32][64]	[32][51][64]		[32]			

2 Problem statement

2.1 Description

The situation considered deals with turbulent flows inside a bi-periodic plane channel with two isothermal walls at different temperatures, as shown in figure [1](#). The corresponding transverse temperature gradient between the cold and hot walls (subscripts 1 and 2, respectively) is characterized by the temperature ratio

$$T_r = \frac{T_2}{T_1}. \quad (2.1)$$

Concerning the dynamic behavior, the flow is characterized by a mean (average) friction Reynolds number based on the friction velocity and the channel half height:

$$\text{Re}_{\tau m} = \frac{\text{Re}_{\tau 1} + \text{Re}_{\tau 2}}{2}, \quad (2.2a)$$

$$\text{Re}_{\tau 1} = \frac{\rho_{w,1} U_{\tau 1} h}{\mu_{w,1}}, \quad (2.2b)$$

$$\text{Re}_{\tau 2} = \frac{\rho_{w,2} U_{\tau 2} h}{\mu_{w,2}}, \quad (2.2c)$$

with $\rho_{w,i}$ and $\mu_{w,i}$ the density and dynamic viscosity at wall i , *i.e.* computed with the temperature corresponding to this wall, and $U_{\tau i}$ the associated friction velocity, obeying the standard relation:

$$U_{\tau} = \sqrt{\frac{\tau_w}{\rho_w}}, \quad (2.3a)$$

$$\tau_w = \mu_w \left. \frac{d\bar{U}}{dy} \right|_w. \quad (2.3b)$$

The bulk and mean variables obey the following definitions:

$$\text{Re}_b = \frac{\rho_b U_b h}{\mu_b}, \quad (2.4a)$$

$$U_b = \frac{1}{2h} \int \bar{U}(y) dy, \quad (2.4b)$$

$$T_m = \frac{1}{2h} \int \bar{T}(y) dy. \quad (2.4c)$$

where the overbar denotes Favre averaging.

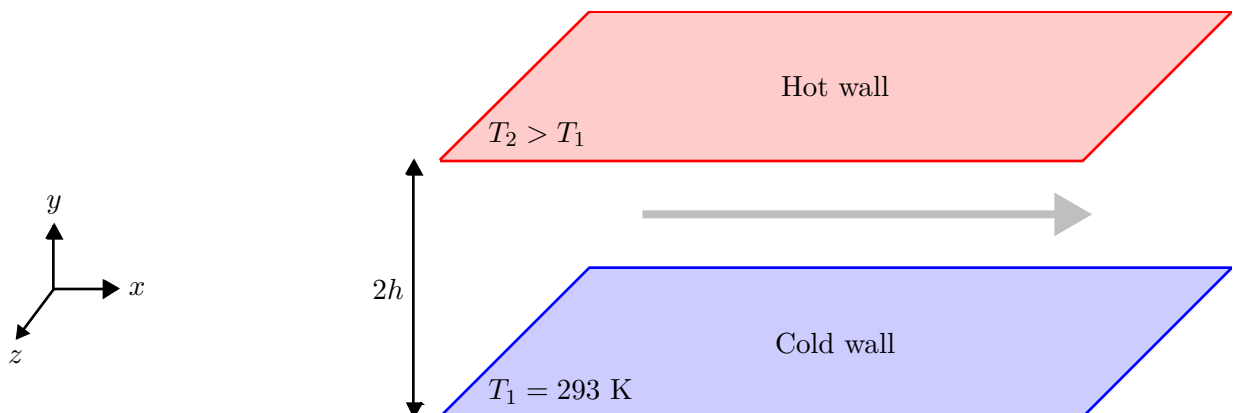


Figure 1 – Description of the configuration

Here, it is worth pointing out that the choice for the definition (2.2a) of an average friction Reynolds number follows former studies on this topic [32, 46, 49, 50]. Nonetheless, such a definition is not unequivocal and one could also use a definition based on a mean viscous stress (*i.e.* on the mean pressure gradient) and on the corresponding mean friction velocity:

$$\tau_{wm} = \frac{\tau_{w1} + \tau_{w2}}{2}, \quad (2.5a)$$

$$U_{\tau m} = \sqrt{\frac{\tau_{wm}}{\rho_b}}. \quad (2.5b)$$

Then, the mean turbulent Reynolds number can be written:

$$\text{Re}_{\tau M} = \frac{\rho_b U_{\tau m} h}{\mu_b}, \quad (2.6)$$

and the two definitions are linked through the following relation:

$$\text{Re}_{\tau M} = \frac{1}{\mu_b} \sqrt{\frac{\rho_b}{2} \left(\frac{\mu_{w1}^2 \text{Re}_{\tau 1}^2}{\rho_{w1}} + \frac{\mu_{w2}^2 \text{Re}_{\tau 2}^2}{\rho_{w2}} \right)}. \quad (2.7)$$

Finally, this enables the mean friction Reynolds number to be plotted as a function of the average value, as shown in figure 2. With respect to Eq. (2.7), there exists a linear relation between these latter two definitions:

$$\text{Re}_{\tau M} = a \text{Re}_{\tau m} + b. \quad (2.8)$$

The various values for the correlation parameters, for all closures and as a function of the temperature ratio, are provided in Table 3. Through this relation, it will thus be possible to extrapolate all the results and conclusions, whatever the definition used for the mean friction Reynolds number.

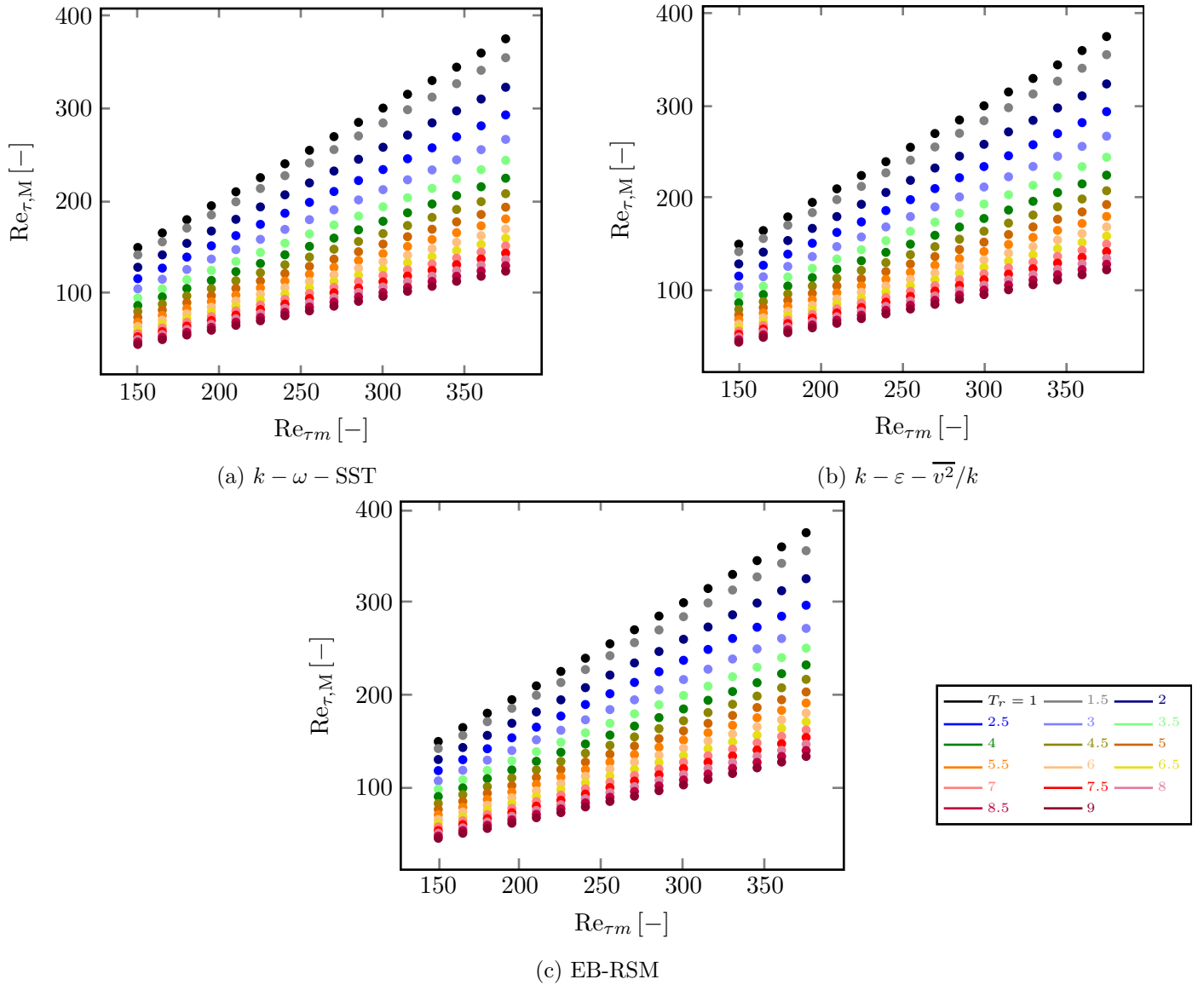


Figure 2 – Mean turbulent Reynolds number as a function of the average turbulent Reynolds number for various temperature ratios

Table 3 – Coefficients of the linear correlation (2.8) for the mean turbulent Reynolds number Re_{τ_M} as a function of the average mean turbulent Reynolds number Re_{τ_m}

T_r	$k - \omega - \text{SST}$		$k - \varepsilon - \overline{v^2}/k$		EB-RSM	
	a	b	a	b	a	b
1	1.001	-0.419	1.001	-0.15	1.001	-0.312
1.5	0.948	-0.382	0.949	-0.482	0.95	-0.181
2	0.866	-1.534	0.87	-2.211	0.869	-0.29
2.5	0.788	-2.641	0.793	-3.682	0.795	-1.398
3	0.718	-3.298	0.725	-4.776	0.73	-2.192
3.5	0.66	-4.139	0.665	-5.311	0.676	-3.106
4	0.611	-4.962	0.615	-6.146	0.63	-4.145
4.5	0.568	-5.372	0.571	-6.762	0.593	-5.591
5	0.53	-5.839	0.533	-6.962	0.562	-7.587
5.5	0.497	-6.13	0.499	-7.218	0.535	-9.345
6	0.469	-6.584	0.47	-7.592	0.511	-10.968
6.5	0.444	-7.13	0.443	-7.656	0.49	-12.483
7	0.422	-7.418	0.42	-7.814	0.469	-13.555
7.5	0.402	-7.93	0.398	-7.918	0.449	-14.457
8	0.384	-8.194	0.38	-8.116	0.429	-14.746
8.5	0.367	-8.319	0.363	-8.475	0.412	-15.169
9	0.352	-8.514	0.348	-8.645	0.395	-15.332

2.2 Modeling

The present situation deals with the flow of a Newtonian fluid, where the hydrostatic pressure has been subtracted from the momentum equation since the flow is in the forced convection regime [28], the maximum value for the bulk Richardson number being 0.0091. Concerning the physical properties, the density and the dynamic viscosity and the thermal conductivity are assumed to vary with the temperature, while the specific capacity and Prandtl number are assumed constant.

In such a case, it has been shown that the low-Mach-number approximation can be applied [28, 32, 44, 49, 51, 66, 67] and this approach was therefore adopted in the present study. Furthermore, it has also been shown that heat transfer is mainly due to forced convection and; natural convection is therefore neglected. In summary, the corresponding system of partial differential equations writes, in the Favre averaging framework, and neglecting the turbulent fluctuations of molecular viscosity and thermal conductivity, as usual,

$$\frac{\partial \rho}{\partial t} + \frac{\partial \rho \bar{U}_i}{\partial x_i} = 0, \quad (2.9a)$$

$$\rho \frac{\partial \bar{U}_i}{\partial t} + \rho \bar{U}_j \frac{\partial \bar{U}_i}{\partial x_j} = -\frac{\partial \overline{P_{\text{dyn}}}}{\partial x_i} + \frac{\partial}{\partial x_j} \left[\mu \left(\frac{\partial \bar{U}_i}{\partial x_j} + \frac{\partial \bar{U}_j}{\partial x_i} \right) \right] - \frac{2}{3} \frac{\partial}{\partial x_j} \left(\mu \frac{\partial \bar{U}_j}{\partial x_j} \right) - \frac{\partial \rho \overline{U'_i U'_j}}{\partial x_j}, \quad (2.9b)$$

$$\rho c_p \frac{\partial \bar{T}}{\partial t} + \rho c_p \bar{U}_i \frac{\partial \bar{T}}{\partial x_i} = \frac{\partial \overline{P_{\text{therm}}}}{\partial t} + \bar{U}_i \frac{\partial \overline{P_{\text{therm}}}}{\partial x_i} + \frac{\partial}{\partial x_i} \left(\lambda \frac{\partial \bar{T}}{\partial x_j} \right) - \frac{\partial}{\partial x_i} \left(\rho c_p \overline{U'_i T'} \right), \quad (2.9c)$$

with P_{dyn} and P_{therm} the dynamic and the thermodynamic pressures (the former being constant in space). The closure of system (2.9) is done by defining the equation of state, here the classical perfect gas law:

$$\overline{P_{\text{therm}}} = \rho R \bar{T}. \quad (2.10)$$

Concerning the other physical parameters, the heat capacity and the Prandtl number are assumed constant, whereas the mean dynamic viscosity and thermal conductivity are assumed to obey Sutherland's law:

$$\bar{\mu} \approx \mu(\bar{T}) = 1.461 \cdot 10^{-6} \frac{\bar{T}^{1.5}}{\bar{T} + 111}, \quad (2.11a)$$

$$\bar{\lambda} \approx \bar{\mu} \frac{c_p}{\text{Pr}} = \frac{1.468 \cdot 10^{-3}}{\text{Pr}} \frac{\bar{T}^{1.5}}{\bar{T} + 111}. \quad (2.11b)$$

In the present study, RANS modeling relies on three different approaches: i) the most recent version of the $k - \omega - \text{SST}$ model [68], ii) the $k - \varepsilon - \bar{v}^2/k$ eddy-viscosity model [59], and iii) the EB-RSM [61]. The first two models are eddy-viscosity models, based on the standard Boussinesq relation and consequently involve a turbulent viscosity, whereas the EB-RSM solves completely the Reynolds-stress tensor transport equations. Both the $k - \varepsilon - \bar{v}^2/k$ and EB-RSM use an elliptic blending approach in order to migrate from a far-field model to a near-wall model. A complete description of all these models is beyond of scope of the present article and the interested reader is referred to [28]. However, the complete set of equations for each model is given in appendices B.1 to B.3

Lastly, the turbulent heat flux is modeled using the SGDh and the GGDh approaches for the first-moment and second-moment closures respectively:

$$\rho \overline{U'_i T'} = -\frac{\mu_t}{\text{Pr}_t} \frac{\partial \bar{T}}{\partial x_i}, \quad (2.12a)$$

$$\rho \overline{U'_i T'^2} = -C_\theta \rho \frac{k}{\varepsilon} \overline{U'_i U'_j} \frac{\partial \bar{T}}{\partial x_j}, \quad (2.12b)$$

with $\mu_t = C_\mu \rho k^2 / \varepsilon$, and $C_\mu = 0.09$, and $\text{Pr}_t = 1$; and $C_\theta = 0.22$.

Finally, the current computations were performed with the finite-volume open-source CFD code Code_Saturne [69], using a second order linear upwind (SOLU) scheme for the convective terms, an iterative reconstruction combined with an arithmetic interpolation for the diffusive and gradient terms, and an implicit Euler integration. The standard SIMPLEC algorithm was used for the pressure-velocity coupling.

Since a dissymmetry appears on the velocity profile, a non-symmetric mesh was used to obtain $y^+ \approx 1$ on both the cold and hot walls so as to have a good description of the associated viscous sublayers. Therefore, the mesh was built in three steps [28]: i) the first zone is composed of regular cells for the low-Reynolds number regions ($y^+ < 20$) near each wall, ii) the second zone is composed of irregular cells obeying a geometrical expansion in order to gradually coarsen the mesh, iii) the third zone is composed of regular cells connecting the second zones of both sides. Following the results of a former grid study [28], the most stringent conditions are for the highest ratios and, consequently the calculations are done with a 230 cells mesh.

Practically, periodicity in the streamwise direction is enforced by adding a source term β to the linear momentum equation (2.9b) in order to account for the constant streamwise pressure gradient:

$$\beta = -\frac{\partial P_{\text{dyn}}}{\partial x} = \frac{\tau_{w1} + \tau_{w2}}{2h}, \quad (2.13)$$

the value of β being iteratively obtained during the computation so as to target a certain friction Reynolds number $\text{Re}_{\tau m}$.

3 Results

In the present case, the half-height of the channel h was set to 0.015 m and, given the aforementioned objectives, a large range of turbulent Reynolds numbers and temperature ratios were tested, namely $\text{Re}_{\tau m}$ ranging from 150 to 375 with an interval of 15 and T_r from 1 to 9 with a 0.5 gap. The maximum value for $T_r = 9$ (also studied in [31] but only for $\text{Re}_{\tau m} = 180$) leads to a temperature of 2637 K. Such a high temperature could in fact be attained in very specific applications in the future, *e.g.* concentrated solar technologies or cooling channels of advanced (fusion) reactors. As mentioned in [70], a large number of articles focus on materials able to resist to very high temperature for solar applications. Some specific solar simulators are already developed in order to achieve very high temperature to test these new receivers. For example, a solar simulator has been developed in PSA – CIEMAT with a peak flux ratio of 1900 kW m^{-2} , which is able to provide a maximum temperature of 2400 K at the aperture [71, 72]. Another solar simulator with a higher peak power output of 75 kW was also designed and developed by ETH Zurich with peak flux ratio of 4250 kW m^{-2} . This simulator can increase the temperature at the aperture up to 3000 K [73]. Furthermore, this value makes it possible to know, from a theoretical point of view, for which value of $\text{Re}_{\tau m}$ it is not anymore necessary to take care about the relaminarization effect. The RANS modeling made it possible to carry out, with a relatively low computation cost, a painstaking analysis covering 816 calculations, for which the incompressibility assumption was systematically checked since the Mach number is always lower than 10^{-2} .

To analyze the results, the velocity and temperature profiles are normalized as follows:

$$U^+ = \frac{\bar{U}}{U_\tau}, \quad (3.14)$$

and

$$T^+ = \frac{\bar{T} - T_w}{T_r}, \quad (3.15a)$$

$$T_r = \frac{\lambda_w \left. \frac{d\bar{T}}{dy} \right|_w}{\rho_w c_p U_\tau}. \quad (3.15b)$$

The first result to be shown directly concerns the evolution of the Nusselt number, which is computed using the half-height of the channel as a characteristic length for the hydraulic diameter definition. Then, to highlight the strong decrease, the final values are compared with an approximated asymptote, which corresponds to infinite plates at (the same) uniform temperature (while there are two temperatures imposed here). With the previous definition of the characteristic length, the classic value of 7.514 becomes 1.885 in the present case. Figure 3 presents the corresponding graphs for the various friction Reynolds numbers and for increasing temperature ratios. Two important features need to be underlined here. Firstly, the behavior is singularly different between the cold and the hot side, since the former shows an almost constant Nusselt number or at least a Nusselt number weakly affected by the temperature ratio, independent of the friction Reynolds numbers. On the contrary, on the hot side, a strong decrease in the Nusselt number is observed for increasing temperature ratios and for all turbulent Reynolds numbers. Secondly, laminarization eventually occurs such that the heat transfer can be reduced by 80% of its initial value.

This last point can also be clearly demonstrated when looking at the evolution of the turbulent viscosity, which is depicted in figure 4. For the eddy-viscosity models, the turbulent viscosity is an intrinsic and important parameter of the models, defined by Eqs. (B.21a) and (B.23) for $k - \omega - SST$ and $k - \varepsilon - \overline{v^2}/k$ respectively. In contrast, the EB-RSM does not use any turbulent viscosity to compute the Reynolds stress. However, to perform comparisons with the previous two closures, an equivalent turbulent viscosity is calculated ex-post as follows:

$$\mu_t^{\text{eq-EBRSM}} = -\frac{\rho \overline{U_1' U_2'}}{\frac{d\overline{U_1}}{dy}} \quad (3.16)$$

For the highest temperature ratio, it is obvious to note that the turbulent viscosity is highly diminished on the hot side. Moreover, this decrease is greater for the lower turbulent Reynolds number. Logically, when looking at the normalized velocity U^+ and normalized temperature T^+ as a function of the non-dimensional distance to the wall, in figures 5 and 6, these effects can be seen as well as their consequence: the higher the temperature ratio, the larger the dissimilarities of the velocity and temperature profiles between the cold and hot walls. Furthermore, such a phenomenon is even more pronounced for the lower $Re_{\tau m}$ (this latter remark also holds for the rest of the analysis). Thus, on the hot side, large deviations from the isothermal case occur; for instance, one can see a departure from the log-law towards the bottom and the top for U^+ and T^+ respectively, in agreement with former observations [19, 32, 74]. This effect seems to be slightly more blatant for U^+ with the $k - \omega - SST$ model than with the two elliptic blending models. This conclusion on the turbulence model no longer holds when considering the T^+ profiles. Here, the curves given by the $k - \omega - SST$ model are closer than those of the two elliptic blending models. When turning to the cold wall, it is noteworthy that the flow is less influenced, which makes sense since here, the conditions are close to the isothermal ones. Nonetheless, even if the effects of the transverse temperature gradient are limited, they can already be clearly seen, specifically for the $k - \varepsilon - \overline{v^2}/k$ results (for both the velocity and the temperature). Lastly, Figure 7 also demonstrates the strong impact of the temperature and the temperature ratio on the density, which, by comparison to the isothermal case, decreases between the cold and hot sides. This first effect is normal due to temperature dependency of the density. More importantly, one can see that for $T_r \leq 4$, the decrease is relatively smooth, yet with a steep fall close to the hot wall. Upon this point, it appears that density decreases very quickly from the cold wall, and then undergoes a smooth and regular reduction. Finally, by combining Figures 6 and 7 it can be observed that the steep density profile close to the cold wall is linked to a turbulent temperature profile, undergoing strong variations. In contrast, at the hot side, the profile is seen to be less steep, emphasizing a local laminar regime.

Therefore, this decrease in the Nusselt number due to laminarization needs to be further analyzed, since it is known that reduction of the heat transfer can easily provoke over-heating and damage the equipment. It is thus crucial to find a way to discriminate situations where this phenomenon can occur, as a function of the operational conditions, that is to say as a function of the turbulent Reynolds numbers and temperature ratio. Consequently, to elucidate the influence of the temperature ratio, it is now proposed to have a look at the overall behavior of the flow, and especially at the evolution of the dynamical parameters. Concretely, the aim will be to search for a possible criterion allowing to predict the conditions where a reverse transition, and so a

fall down of heat transfer, can arise.

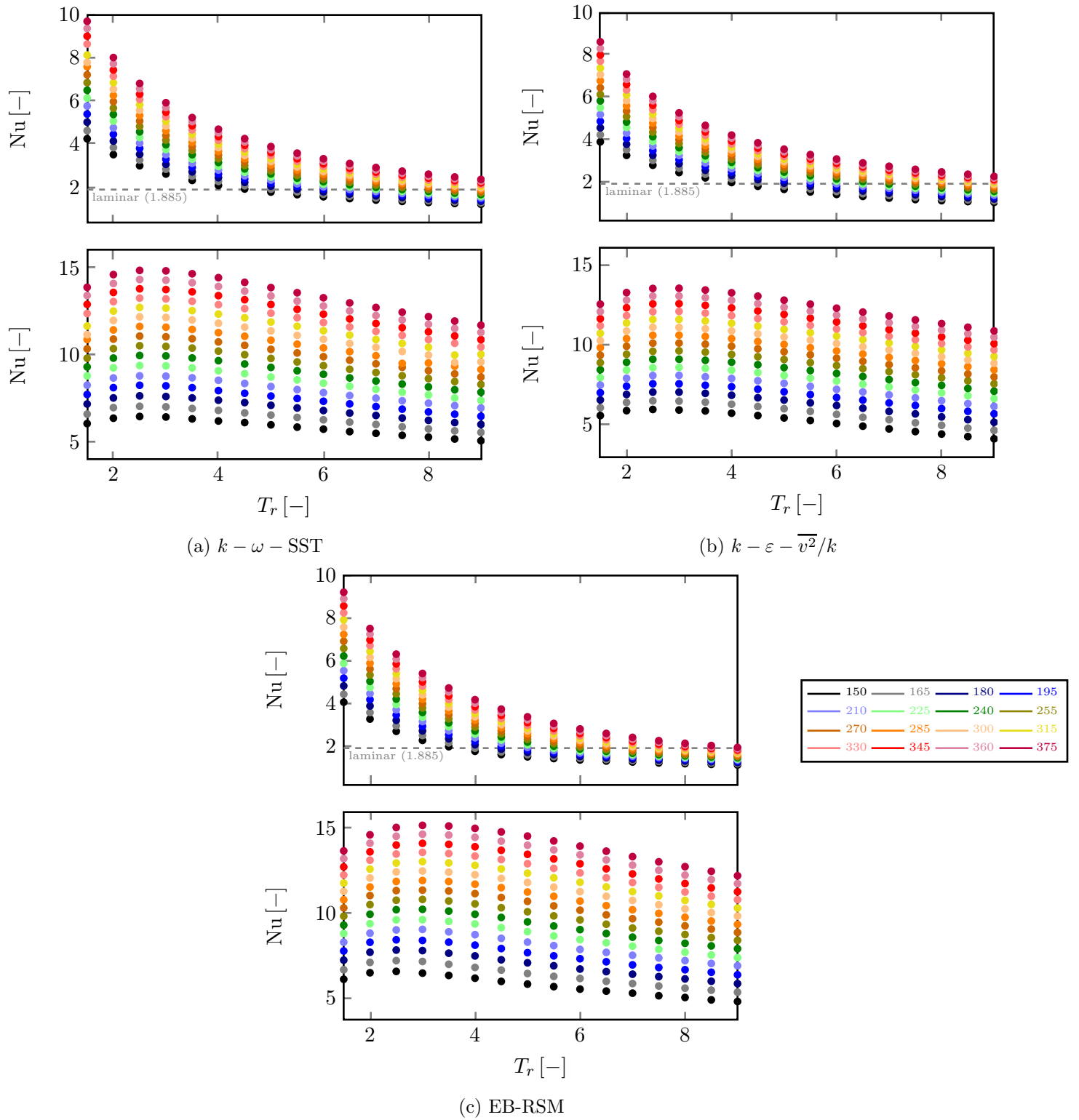


Figure 3 – Nusselt number on the cold (bottom) and hot (top) walls as a function of the temperature ratio for various turbulent Reynolds numbers

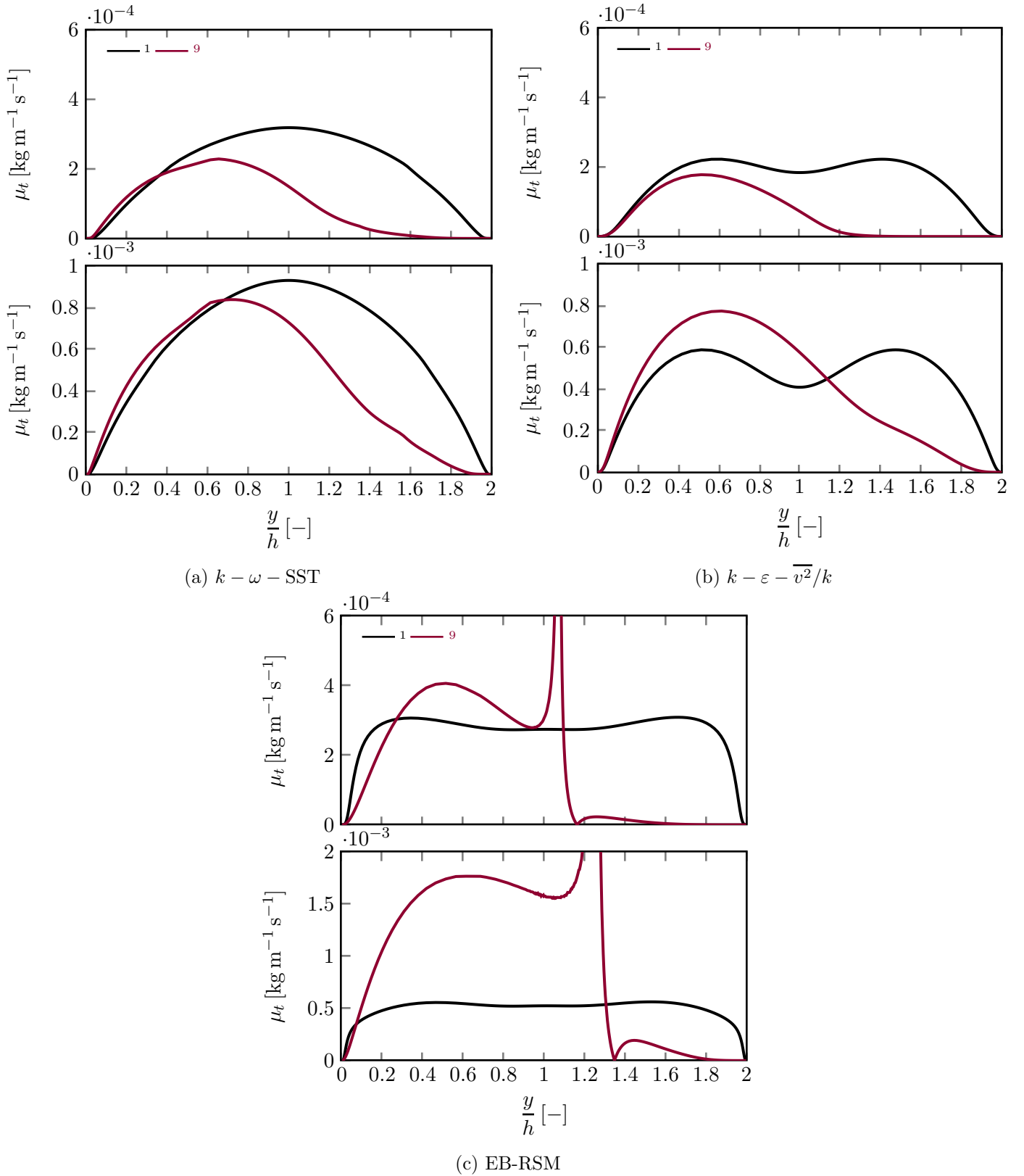
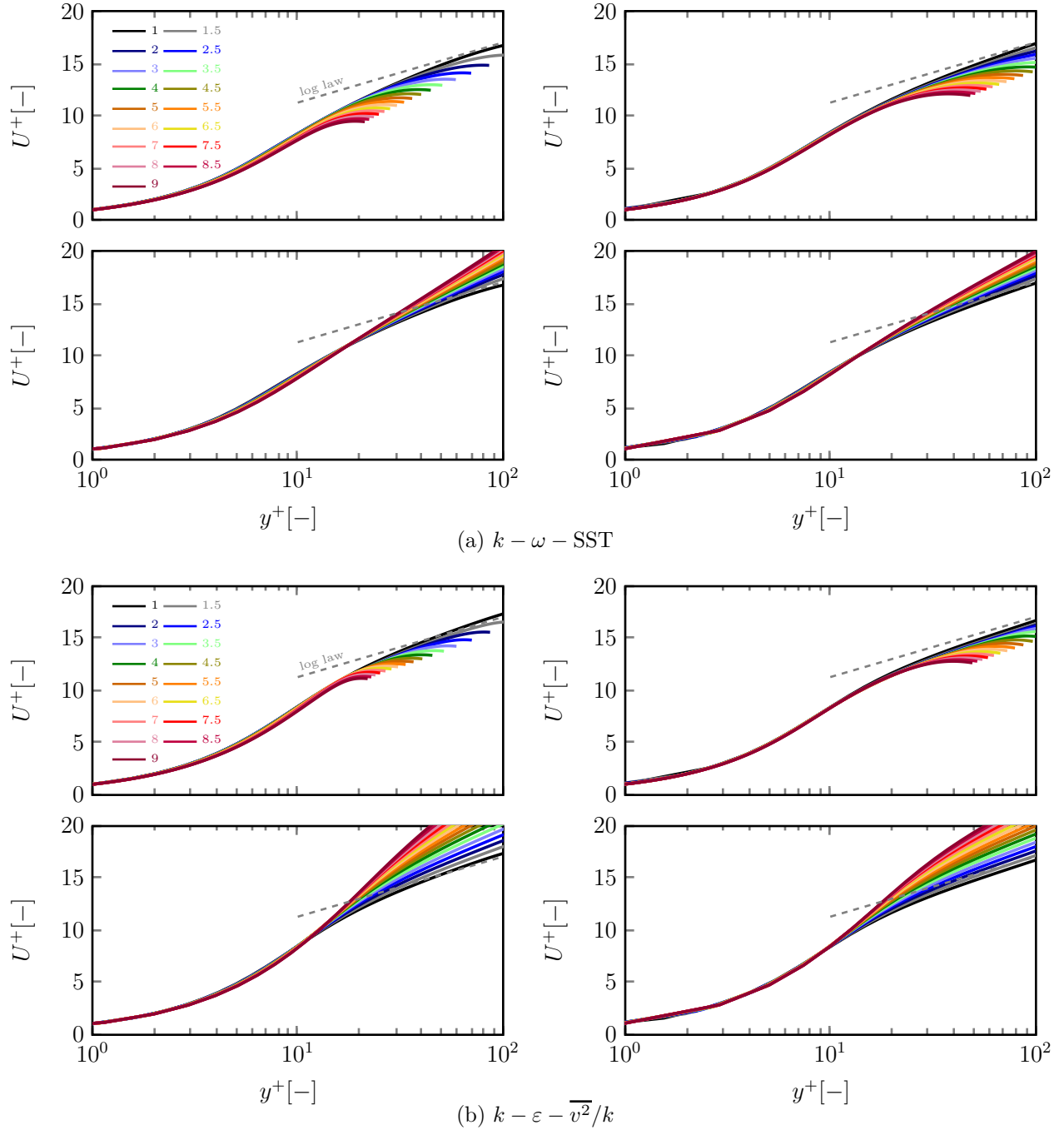


Figure 4 – Turbulent viscosity as a function of the non-dimensional distance to the cold wall for two temperature ratios ($T_r = 1$ and 9) for the various RANS results for the lowest ($\text{Re}_{\tau_m} = 150$, top) and highest ($\text{Re}_{\tau_m} = 375$, bottom) turbulent Reynolds numbers

Figure 5 – Non-dimensional velocity U^+ on the hot (top) and cold (bottom) walls as a function of y^+ for the minimum and maximum turbulent Reynolds numbers, $Re_{\tau_m} = 150$ (left side) and $Re_{\tau_m} = 375$ (right side), for various temperature ratios



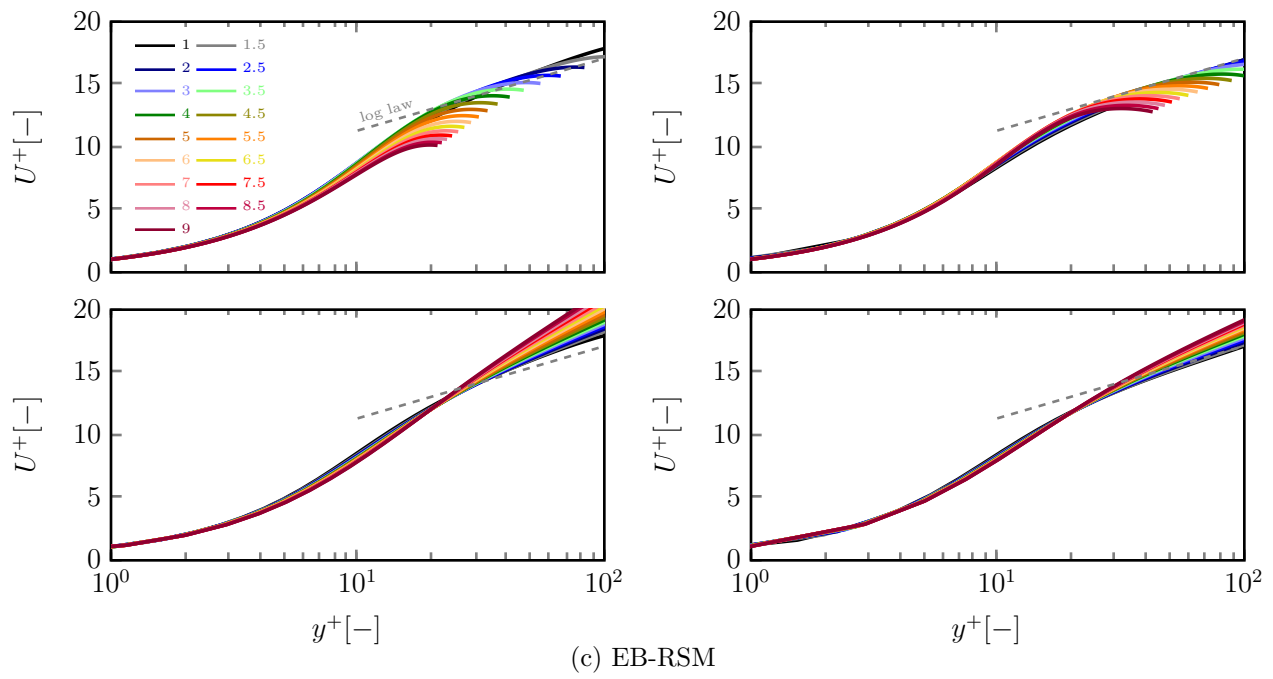
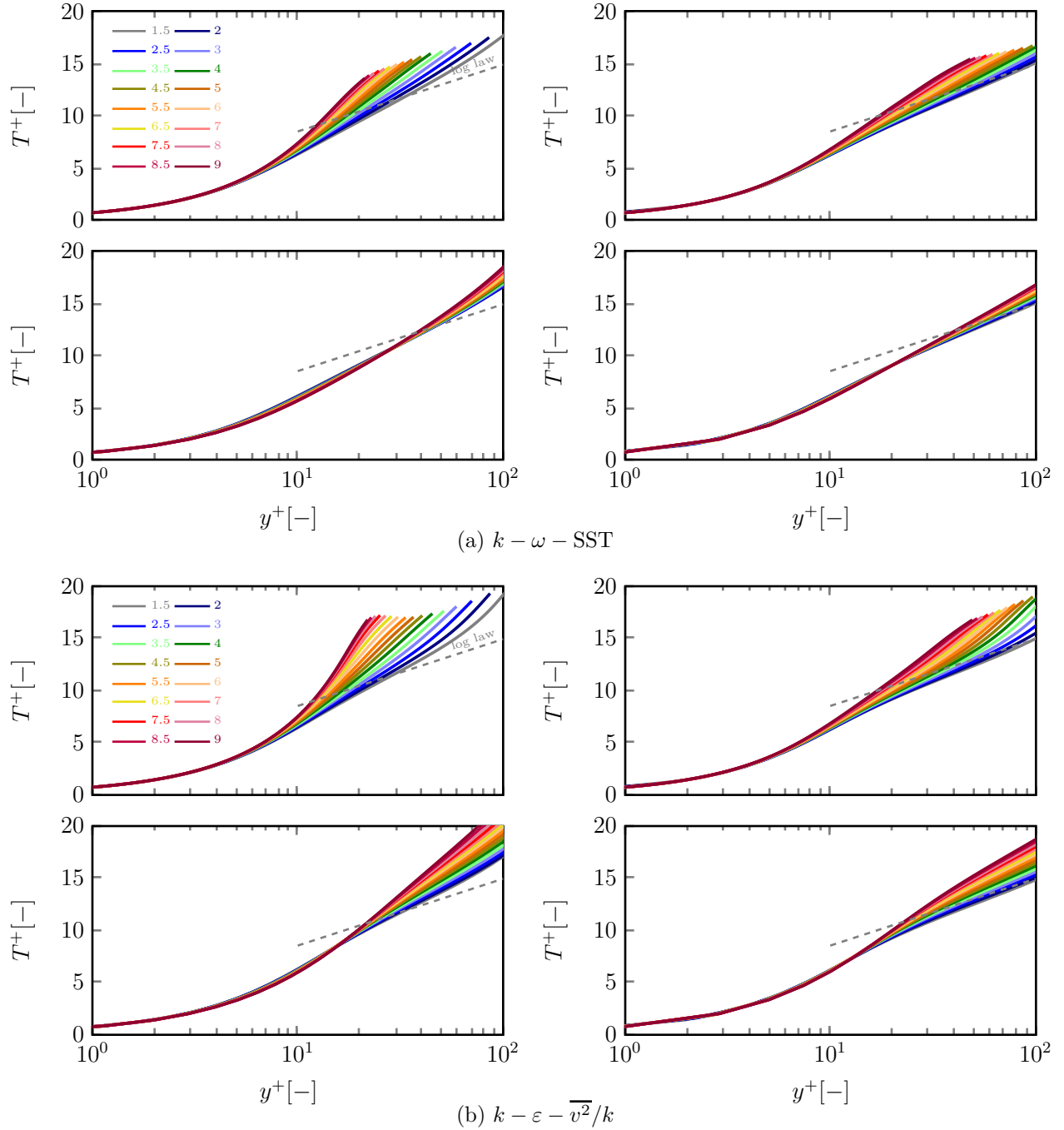
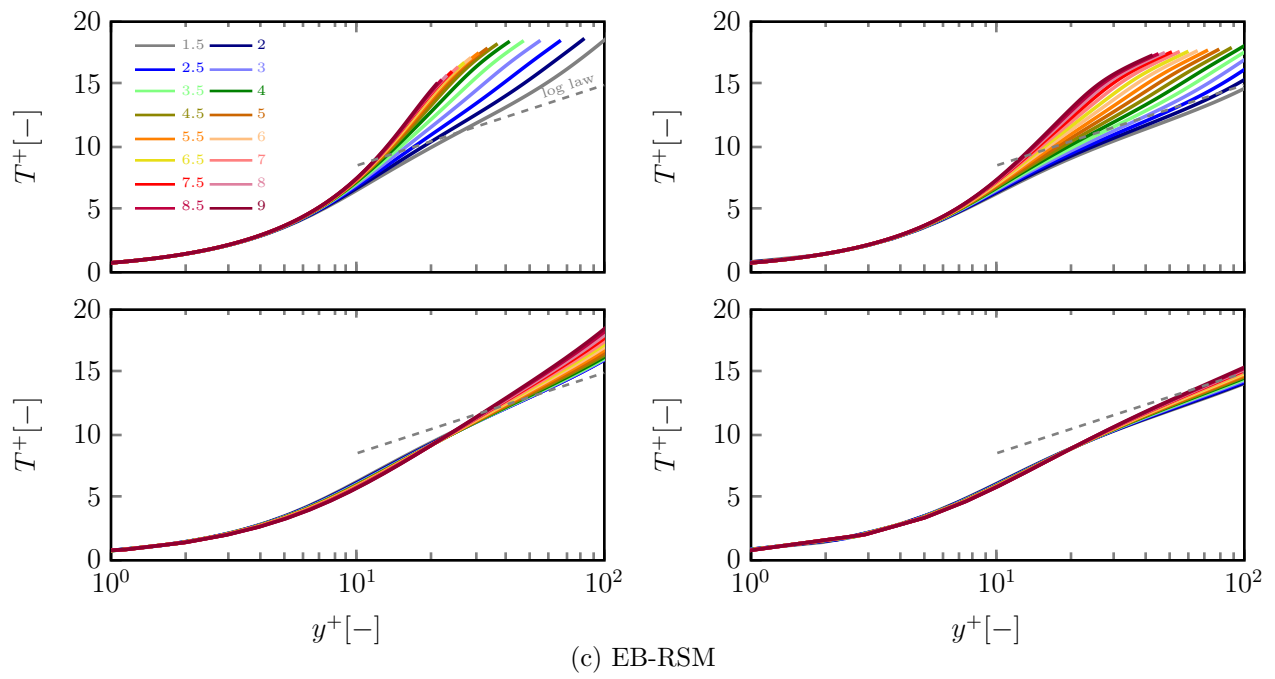


Figure 6 – Non-dimensional temperature T^+ on the hot (top) and cold (bottom) walls as a function of y^+ for the minimum and maximum turbulent Reynolds numbers, $\text{Re}_{\tau_m} = 150$ (left side) and $\text{Re}_{\tau_m} = 375$ (right side), for various temperature ratios





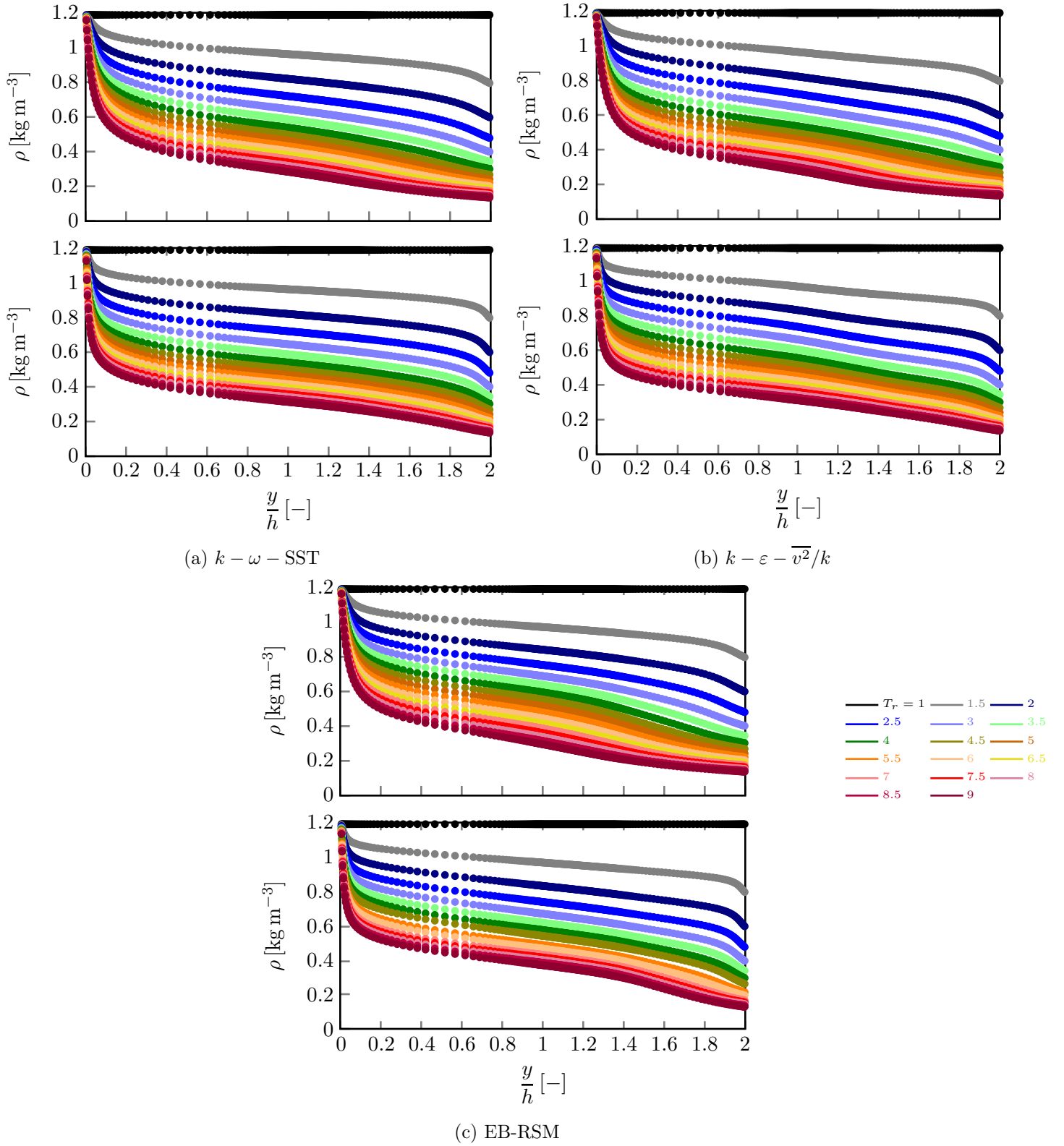


Figure 7 – Density as a function of the non-dimensional distance to the cold wall for the various temperature ratios for the lowest ($Re_{\tau_m} = 150$, top) and highest ($Re_{\tau_m} = 375$, bottom) turbulent Reynolds numbers

The evolution of the bulk Reynolds number (normalized each time by its corresponding isothermal value) with the temperature ratio is depicted in figure 8 as well as the average friction Reynolds number as a function of the bulk Reynolds number in figure 9; as already mentioned, simulations were validated with DNS and/or LES data for the available temperature ratios 28. It can be clearly seen that Re_b decreases strongly with increasing temperature ratios. Furthermore, this trend is almost similar for all the turbulent Reynolds numbers, with an exception for the EB-RSM case. This can be explained by the fact the EB-RSM model solves the transport equations and does not use the Boussinesq hypothesis, unlike the other two models. In the latter case, as the decrease in the bulk Reynolds number is slightly less pronounced, the laminarization should occur later for the higher turbulent Reynolds numbers. Then, it can be seen that, for a given friction Reynolds number, the bulk Reynolds number decreases with the temperature ratio. In other words, for a similar pressure gradient, or head loss, the flow-rate will be lower. Roughly speaking, the bulk Reynolds number is divided by two around $T_r \approx 4$. Once again, this is in agreement with experimental observations 14 and all models are thus able to reproduce this lower thermal influence for high friction Reynolds numbers.

Finally, since the general features of the flow are greatly modified, it is interesting to focus on the behavior near the walls to see how the flow is affected there. Figure 10 presents the evolution of the friction Reynolds number on the cold and hot sides as a function of the temperature ratio for the various mean friction Reynolds numbers. It is clear that friction Reynolds numbers on both sides show strong variations with the temperature ratio, with an increase near the cold wall, and a decrease on the hot side. It is worth mentioning here that the evolution on the cold side is similar for all mean turbulent Reynolds numbers and all closures, the value being multiplied up to 3 for the highest temperature ratio. However, near the hot wall, the results are slightly different for the various turbulent Reynolds numbers, specifically with the EB-RSM, and are divided by 100 for $T_r = 9$ by comparison with their isothermal case. Moreover, the $k - \omega - SST$ and $k - \varepsilon - \overline{v^2}/k$ models give almost similar results and predict a lower decrease than EB-RSM. Although the flow is fully turbulent, it is thus obvious that these low friction Reynolds number values near the hot wall can lead to laminarization, since it has been suggested that it could occur around $Re_{\tau, a}^* = 63$ for isothermal channel flows 75.

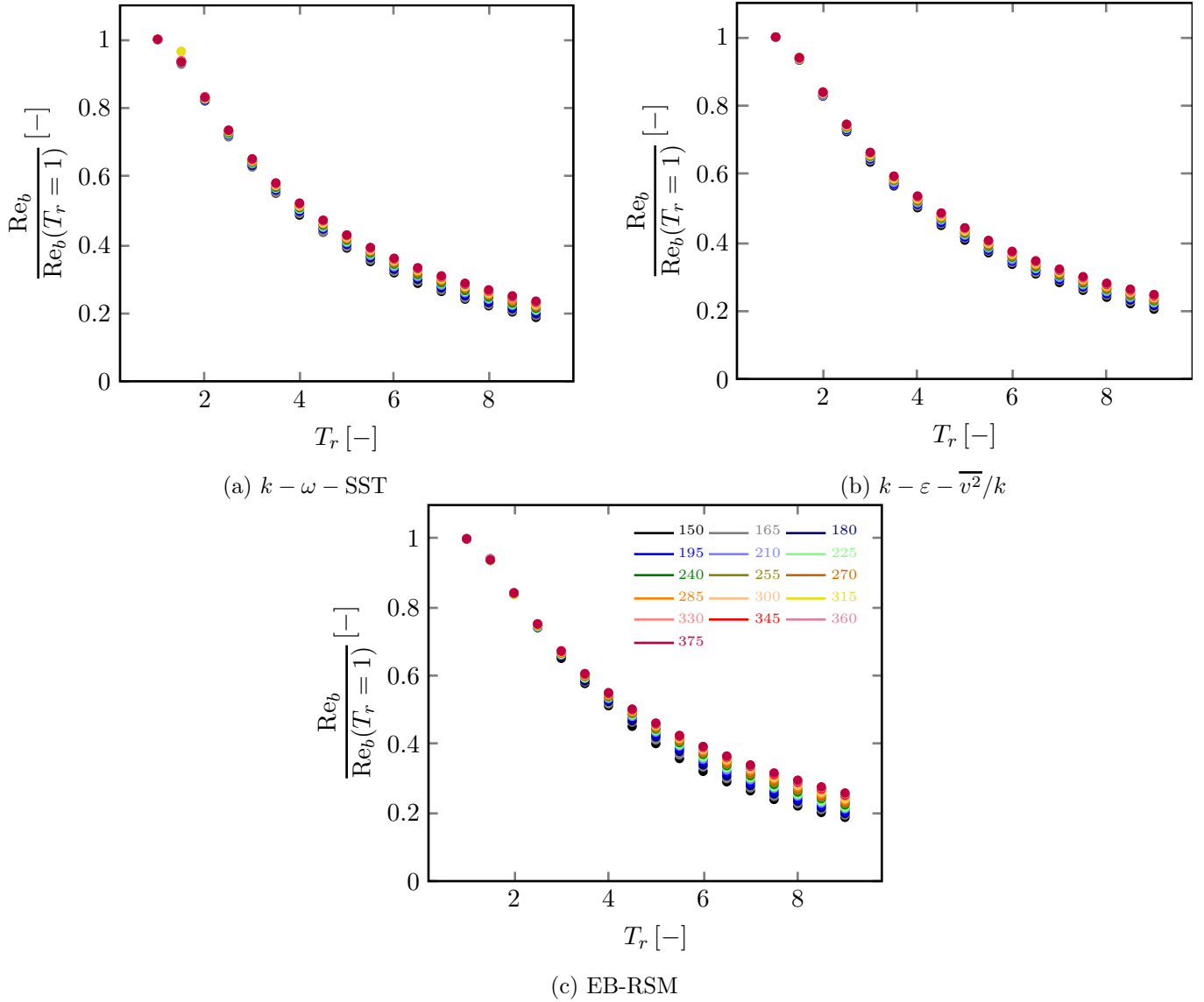


Figure 8 – Normalized bulk Reynolds number as a function of the temperature ratio for various turbulent Reynolds numbers

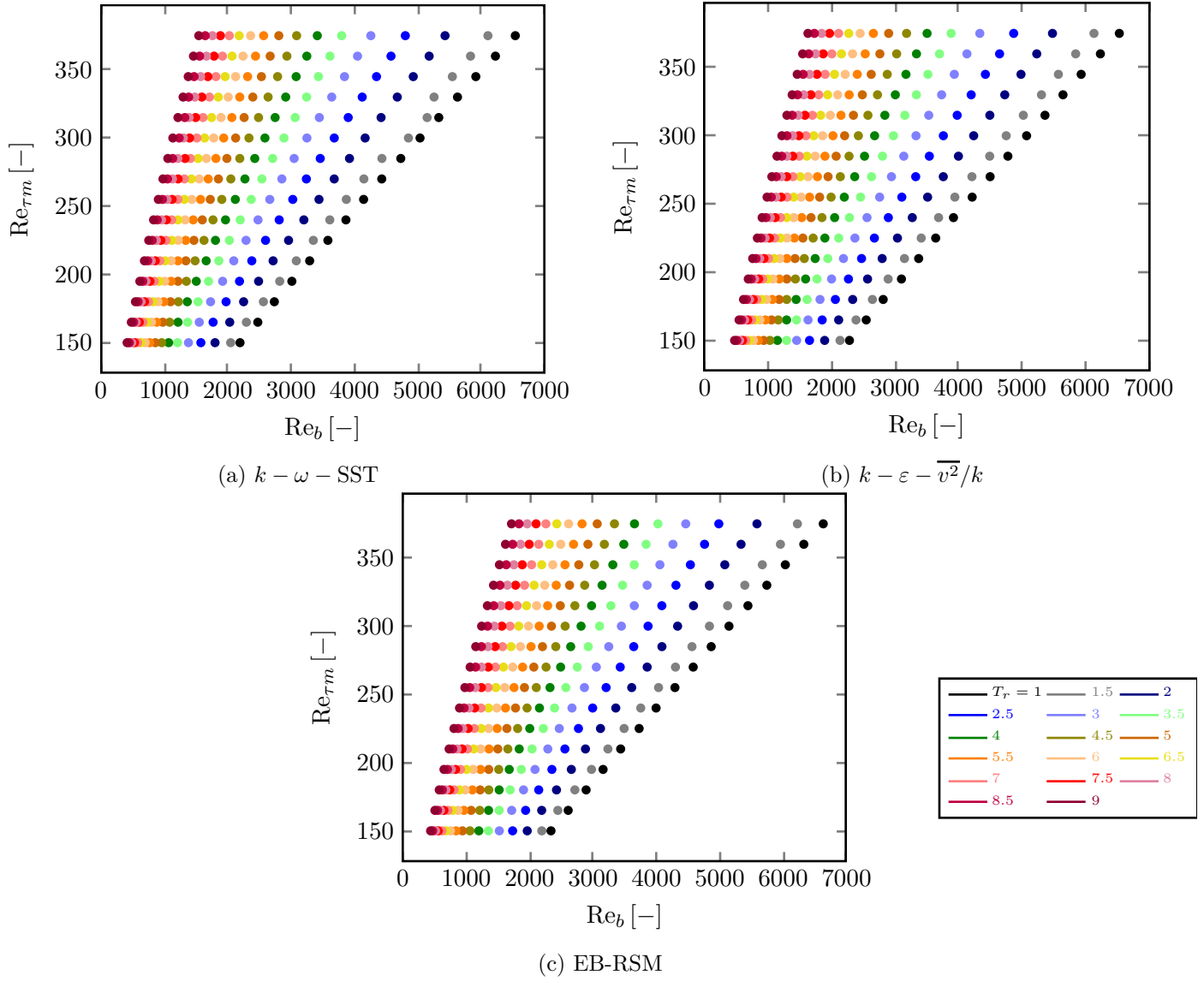


Figure 9 – Average turbulent Reynolds number as a function of the bulk Reynolds number for various temperature ratios

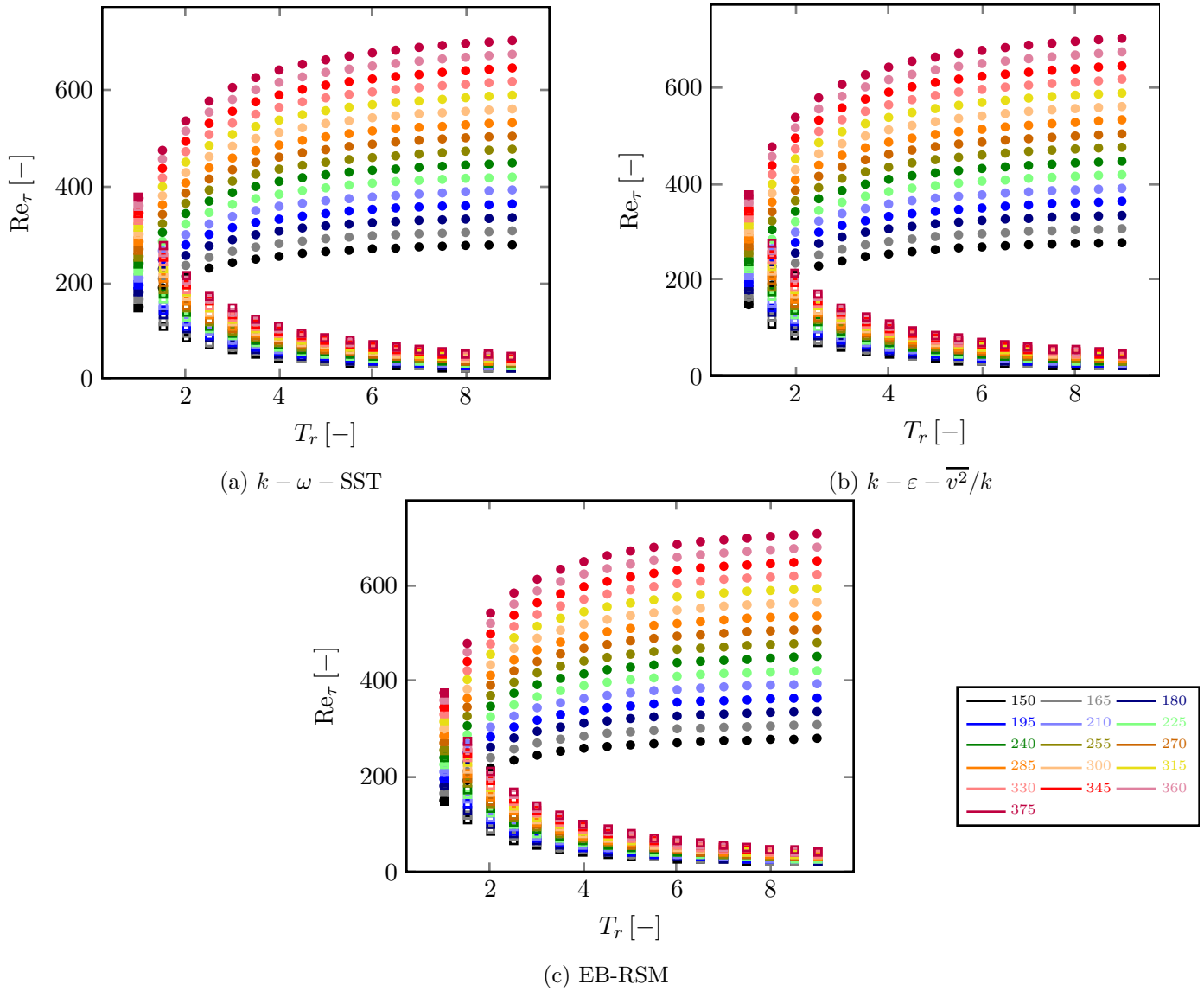


Figure 10 – Friction Reynolds number on the cold (circle) and hot (square) walls as a function of the temperature ratio for various turbulent Reynolds numbers

After showing the predictions for the bulk variables as well as their variations, for the various RANS closures, near the cold and hot walls, it is proposed to turn to the main goal of the present study, namely the reverse transition. Thereinbefore, it has been shown that RANS calculations can qualitatively predict relatively well the physical conditions where laminarization could occur. The next step is logically to search for a quantitative assessment of this occurrence. In fact, the aim is to build and propose guidelines and/or safeguards, which could be used to identify the possible situations of reversion with non-isothermal flows. Put differently, a correlation for the prediction of a laminarized flow, as a function of the friction Reynolds number and the temperature ratio, is searched for. Concretely, two approaches will be developed to handle this problem.

Firstly, it is proposed to recall the above remark concerning the existence of a threshold for the turbulent Reynolds number under which laminarization occurs. To define this lower limit, one can either re-use the numerically obtained value of $Re_\tau^* = 63$ [75], or use the stability analysis of [76] who established that a Hopf bifurcation exists at $Re_b \approx 5772.22$, *i.e.* for a friction Reynolds number value approximately equal to $Re_\tau^* = 186$, which distinguishes the completely unstable and partially stable regimes. Since the reversion should occur on the hot side, it seems logical to look for the moment when the corresponding friction Reynolds number could go below these critical values. In other words, two limiting thresholds for Re_{τ_2} are defined. Furthermore, in the light of the results provided in figure 10 it appears that the friction Reynolds number near the hot side Re_{τ_2} can be expressed as a function of the temperature ratio. Assuming a power-law, this leads to:

$$Re_{\tau_2} = C T_r^n, \quad (3.17)$$

the corresponding parameters being given in Table 4

From Eq. (3.17), it is then easy to compute the two corresponding critical temperature ratios T_r^* associated with the two limiting thresholds $Re_{\tau_2}^*$ for Re_{τ_2} :

$$T_{r,a}^* = \left(\frac{Re_{\tau_2,a}^*}{C} \right)^{1/n} \quad \text{with } Re_{\tau_2,a}^* = 63. \quad (3.18a)$$

$$T_{r,b}^* = \left(\frac{Re_{\tau_2,b}^*}{C} \right)^{1/n} \quad \text{with } Re_{\tau_2,b}^* = 186. \quad (3.18b)$$

Lastly, since the present definition of the mean (average) turbulent Reynolds number has been shown in Eq. (2.8) to be correlated to the mean turbulent Reynolds number, associated with the mean viscous stress, it is proposed to directly plot the results as a function of the latter. The corresponding results are given in Figure 11, where the phase space is divided into three zones. The 'safe' zone holds for situations where the hot friction number is always greater than the severest condition, that is to say the highest possible value given by Eq. (3.18b). On the contrary, the 'forbidden' zone corresponds to conditions where laminarization of the turbulent flow is predicted, whatever the criterion retained. Between these two situations, a 'dangerous' zone is postulated where the reverse transition could occur, either partially or intermittently, or where the current relations are not stringent enough to incontrovertibly establish or exclude this possibility. When looking more carefully at the results, the first remark to be made concerns the relative homogeneity in the prediction for all RANS closures, though the EB-RSM always predicts a larger turbulent zone for higher temperature ratios. The second remark comes from the appearance of the three distinct zones defined above. Depending on $Re_{\tau_2,a}^* = 63$ or $Re_{\tau_2,b}^* = 186$, the acceptable temperature ratios for a given turbulent Reynolds number can greatly vary. Assuming that the temperature ratio is not modifiable, due to physical constraints, and that one can only vary the flow regime, there can be a factor of 4 on the targeted mean friction Reynolds number, which must be set to absolutely avoid any reverse transition. Nevertheless, even if this is also a fundamental constraint, one can now use (even with a safety factor) the present quantitative predictions to ensure that one always remains in the 'safe' zone.

Table 4 – Coefficients of the power correlation (3.17) for the turbulent Reynolds number on the hot wall as a function of the mean turbulent Reynolds number

Re_{τ_m}	$k - \omega - SST$		$k - \varepsilon - \overline{v^2}/k$		EB-RSM	
	C	n	C	n	C	n
150	157.338	-0.912	157.709	-0.904	151.692	-0.915
165	174.133	-0.921	174.187	-0.912	168.385	-0.931
180	190.654	-0.928	190.617	-0.918	185.784	-0.947
195	207.288	-0.933	206.713	-0.922	202.675	-0.958
210	223.449	-0.937	222.809	-0.925	219.452	-0.968
225	240.449	-0.942	238.529	-0.927	236.952	-0.978
240	257.005	-0.945	254.837	-0.931	253.982	-0.985
255	272.98	-0.947	270.855	-0.932	272.027	-0.994
270	289.306	-0.949	287.217	-0.935	289.541	-1
285	305.863	-0.951	303.002	-0.937	306.352	-1.005
300	322.321	-0.953	318.942	-0.938	323.548	-1.009
315	338.745	-0.954	335.197	-0.94	341.261	-1.013
330	355.501	-0.957	351.385	-0.942	358.618	-1.016
345	371.828	-0.958	367.519	-0.944	375.851	-1.019
360	388.438	-0.959	383.638	-0.946	393.227	-1.022
375	404.739	-0.96	399.913	-0.947	410.268	-1.023

Secondly, another approach is going to be discussed, based on former observations on fundamental differences between non-isothermal laminar and turbulent flows with both LES and RANS calculations. In both cases, it has been shown that a dissymmetry in the velocity field occurs under a transverse temperature gradient [27, 32, 66, 77, 79], yet it has also been shown [31, 32] and then demonstrated that this asymmetry elicits a shifting of the position of the velocity maximum towards the cold wall and the hot wall in the laminar and turbulent case respectively [28], as illustrated in figure [12]. Therefore, it is suggested here that a displacement of the velocity maximum towards the cold wall could be a local criterion emphasizing the occurrence of a reverse transition. Using this protocol, the position of the maximum velocity is determined for all cases: the corresponding value is then compared with the reference one, achieved for the position in the isothermal case. Thus, it is possible to compute a displacement of the position where the maximum velocity of the flow is achieved, as shown in figure [13]. Thereby, it is obvious that, for the higher friction Reynolds numbers, the present method does not show any reversion of the flow. Here, it could be conjectured that a further increase in the temperature ratio would lead to laminarization. However, this has not been tested since the last values were already questionable (validity of Sutherland's law) and, more importantly, because this would imply temperatures above 2700 K which are clearly unrealistic for industrial applications. Besides, it is interesting to note that all models undergo the same behavior although the predictions show clear differences. Thus, the EB-RSM always gives a lower value for the position of the maximum where reversion begins: see for instance 225, 240 and 255 where $k - \omega - SST$ and $k - \varepsilon - \overline{v^2}/k$ results present a kind of plateau whereas the EB-RSM ones show a strong decrease. From the determination of these critical values, it is possible to plot them as a function of the friction Reynolds number, as is done in figure [14]. It is remarkable that, except for the $k - \varepsilon - \overline{v^2}/k$, a linear correlation fits these results very well:

$$k - \omega - SST: \quad T_r^* = 0.0217 Re_{\tau_M} + 1.8979 \quad \text{with } R^2 = 0.98875 \quad (3.19a)$$

$$k - \varepsilon - \overline{v^2}/k: \quad T_r^* = 0.0086 Re_{\tau_M} + 4.7771 \quad \text{with } R^2 = 0.94039 \quad (3.19b)$$

$$EB-RSM: \quad T_r^* = 0.0181 Re_{\tau_M} + 1.7204 \quad \text{with } R^2 = 0.99576 \quad (3.19c)$$

As first sight, this new method seems less ambiguous, mainly because the definition of laminarization now relies on a unique criterion. For the sake of generality, the results obtained with this new criterion are plotted and compared with the previous results using a critical threshold on the hot turbulent Reynolds number. The results are shown in dashed lines in Figure [11](#). On the current tested range for the friction Reynolds number, this second method falls between the two extreme values, in the 'dangerous' zone. However, although this method strongly suggests avoiding the region above the dashed line in Figure [11](#), it is worth mentioning that its practical application in industrial systems is difficult since its proper definition relies on the search for an extremum between several different calculations.

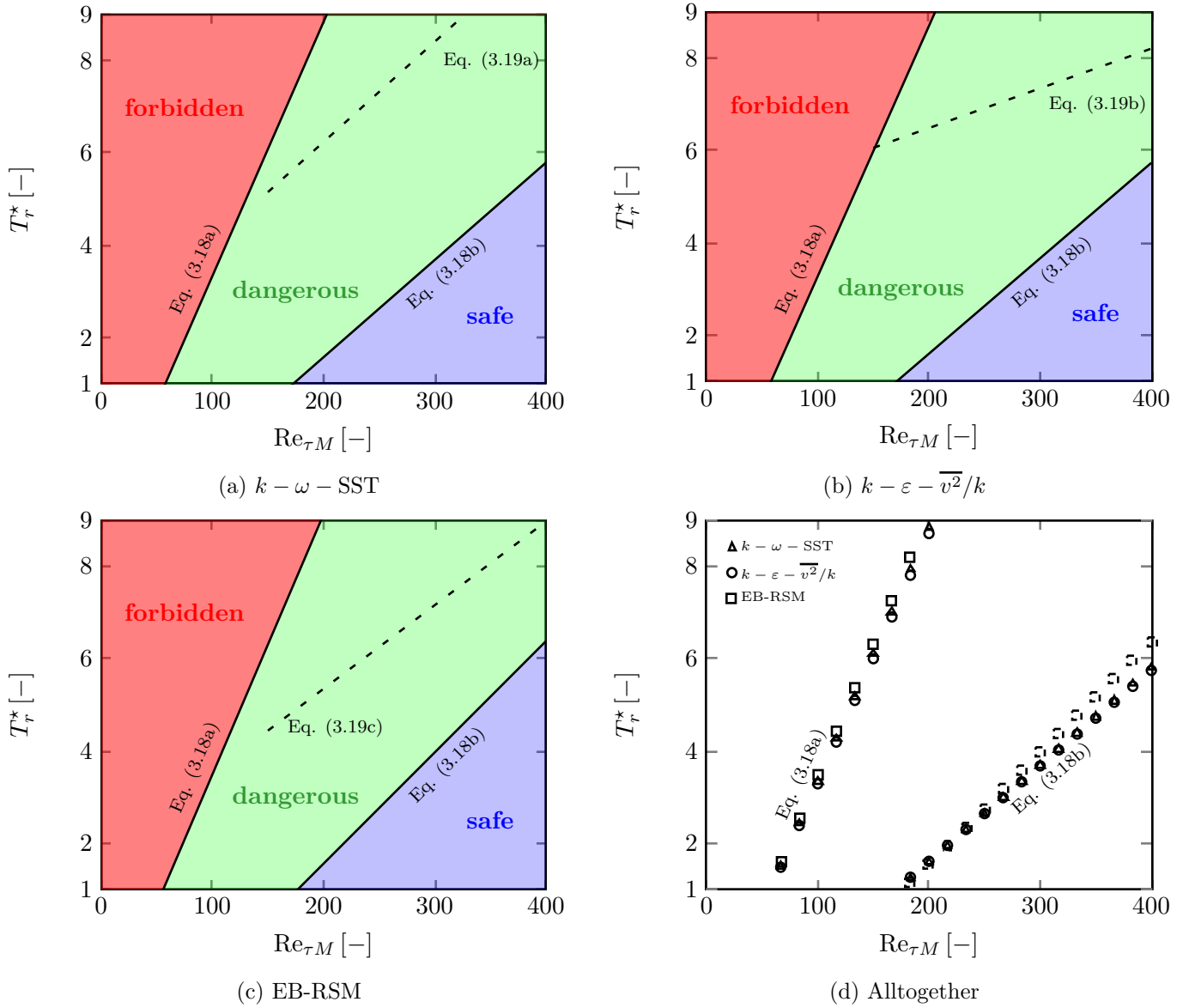


Figure 11 – Separation zones for the friction Reynolds number leading to reverse transition for various critical thresholds

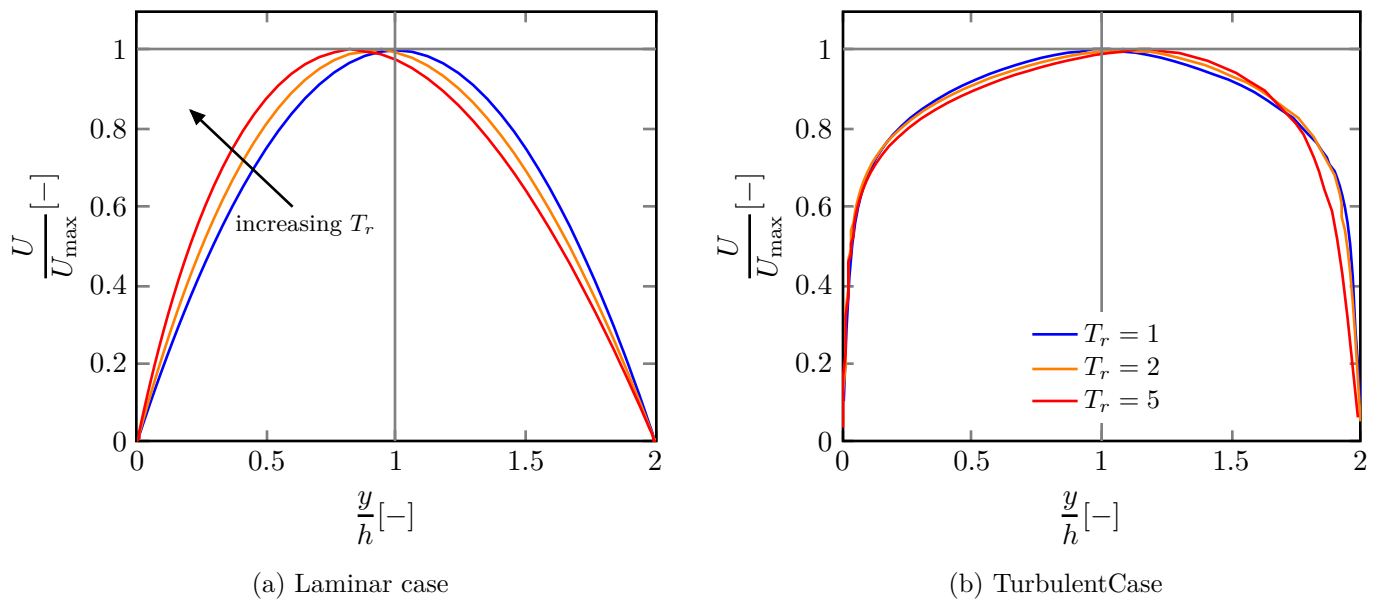


Figure 12 – Velocity profiles for non-isothermal Poiseuille flows

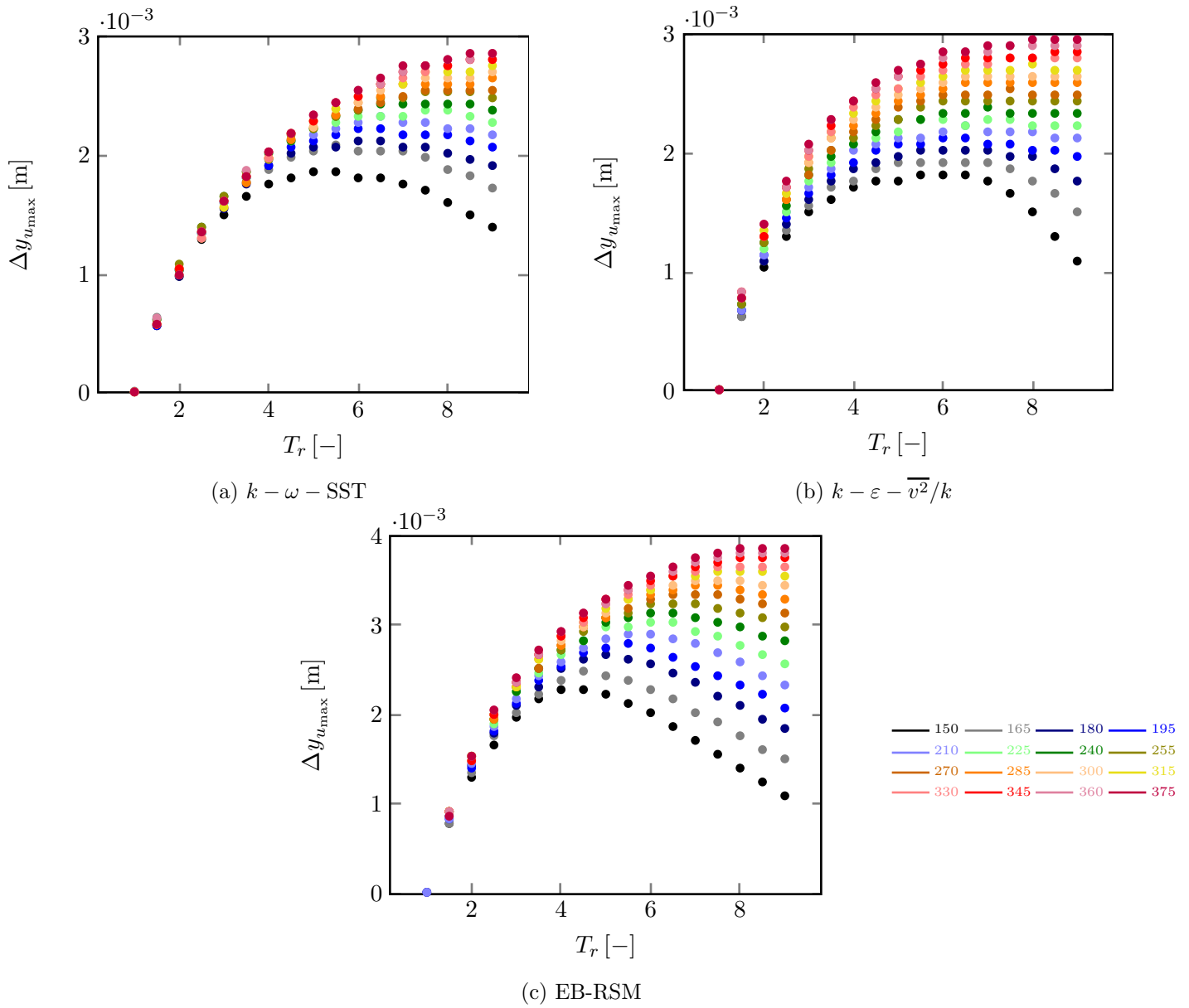


Figure 13 – Vertical shift of the velocity maximum, when compared with the isothermal case, as a function of the temperature ratio for various turbulent Reynolds numbers

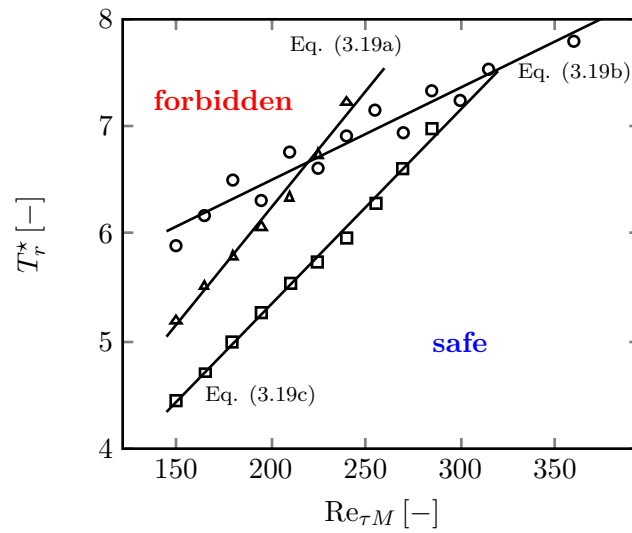


Figure 14 – Critical temperature ratio as a function of the turbulent Reynolds number for the three RANS models: $k - \omega - SST$ (triangle), $k - \varepsilon - \overline{v^2}/k$ (circle), EB-RSM (square)

4 Conclusion

In the present paper, the reverse transition due to transverse temperature gradients of initially turbulent channel flows has been studied with a RANS approach. Physically, the low-Mach number approximation was considered and the physical properties were temperature-dependent. Three RANS closures were tested, relying not on wall functions but on near wall modeling. Both first-moment and second-moment closures are involved, with the $k - \omega - SST$ and the $k - \varepsilon - \overline{v^2}/k$ from one side and the EB-RSM from the other, the latter two also involving an elliptic blending approach. The turbulent heat flux model used is the SGDh and the GGDh in the first and second case, respectively. By performing a painstaking analysis, involving 816 calculations, for various friction Reynolds numbers and temperature ratios between the walls, the onset of laminarization was studied. The use of three different turbulence models makes it possible to assess an order of magnitude of the uncertainty associated with the model and to draw prudent conclusions.

The first and most important conclusion is the prediction of a large decrease in the Nusselt number, which can undergo a variation up to 80%. The turbulent viscosity is also singularly reduced near the hot wall, while the normalized velocity and temperature profiles move away from the standard log-law. Practically, these effects are particularly pronounced for high temperature ratios, especially with the lower friction Reynolds number values. The results also show the ability to predict the diminishing of the bulk Reynolds number, and consequently of the flow-rate for a given pressure gradient, as with former experiments. Then, when looking at the specific evolution of the turbulent Reynolds number near the walls, it logically appears that on the hot side, very low values can be achieved such that reversion can occur. Therefore, it is proposed to define a specific threshold characterizing this laminarization and two values (63 and 186) were tested for the corresponding friction Reynolds number. The first one is based on an observation, and the second one on a fully turbulent state derived from stability analysis. This approach makes it possible to identify, for each friction Reynolds number, a range of temperature ratios in which the reverse transition process occurs. Thus, the operational space parameter is divided into three specific zones: a 'forbidden' one where the flow is laminar (and the heat transfer possibly very low), a 'safe' one where the flow remains turbulent and a 'dangerous' one where there exist some uncertainties. In summary, there is a range of temperature ratios vs. mean pressure gradient that can potentially harm the devices. If one wants to avoid any risk, the application must operate in its 'safe' zone. On the contrary, if one seeks an optimization of the control, the application can be operated in its 'dangerous' zone up to the extremum displacement of the velocity maximum. In spite of these interesting first results, it is also worth recalling two possible weaknesses. First, the conclusions are drawn from RANS calculations, whose predictions are known to be rather model-dependent. This is specifically emphasized by the discrepancies observed between each of the closures; though their qualitative behavior is similar, the quantitative assessment is still questionable. Second, it is still difficult to know, especially with the above-mentioned limitations, what is the unequivocal criterion leading to laminarization.

In the light of these discussions, the need for DNS or LES of turbulent flows with low turbulent Reynolds number values and high temperature ratios is undoubtedly highlighted. Indeed, such simulations could provide reliable data that could be used to validate at least the main trends of the phenomenon. In a near future, it is proposed to characterize such a phenomenon from a practical point of view. For industrial applications, *e.g.* T-junctions with flows at different velocities and temperatures, the computed heat transfer at the walls could be performed in situations similar to the present cases. Among the possible goals, the influence of the temperature-dependency on the flow behavior could be highly interesting.

References

- [1] R. Narasimha and K.R. Sreenivasan. Relaminarization of fluid flows. In Chia-Shun Yih, editor, *Advances in Applied Mechanics*, volume 19, pages 221 – 309. Elsevier, 1979.
- [2] D. M. McEligot, C. W. Coon, and H. C. Perkins. Relaminarization in tubes. *International Journal of Heat and Mass Transfer*, 13(2):431 – 433, 1970.
- [3] J.D. Jackson, M.A. Cotton, and B.P. Axcell. Studies of mixed convection in vertical tubes. *International Journal of Heat and Fluid Flow*, 10(1):2 – 15, 1989.
- [4] Donald M. McEligot. Convective heat transfer in internal gas flows with temperature-dependent properties. Technical report no. 2, Arizona Univ., Tucson, 05 1982.
- [5] Donald M. McEligot and J. Derek Jackson. “Deterioration” criteria for convective heat transfer in gas flow through non-circular ducts. *Nuclear Engineering and Design*, 232(3):327 – 333, 2004.
- [6] C.A. Bankston. The transition from turbulent to laminar gas flow in a heated pipe. *ASME J. Heat Transfer*, 92(4):569–579, 1970.
- [7] C. W. Coon and H. C. Perkins. Transition from the turbulent to the laminar regime for internal convective flow with large property variation. *ASME J. Heat Transfer*, 92(3):506–512, 1970.
- [8] K. R. Perkins, K. W. Schade, and D. M. McEligot. Heated laminarizing gas flow in a square duct. *International Journal of Heat and Mass Transfer*, 16(5):897 – 916, 1973.
- [9] Suichi Torii, Akihiko Shimizu, Shu Hasegawa, and Masaaki Higasa. Laminarization of strongly heated gas flows in a circular tube. *JSME International Journal Series II*, 33(3):538 – 547, 1990.
- [10] Suichi Torii, Akihiko Shimizu, Shu Hasegawa, and Nobuyuki Kusama. Laminarization of strongly heated annular gas flows. *JSME International Journal Series II*, 34(2):157 – 168, 1991.
- [11] Shuichi Torii and Wen-Jei Yang. Laminarization of turbulent gas flow inside a strongly heated tube. *International Journal of Heat and Mass Transfer*, 40(13):3105 – 3117, 1997.
- [12] A. Mohsen Shehata and Donald M. McEligot. Mean structure in the viscous layer of strongly-heated internal gas flows. Measurements. *International Journal of Heat and Mass Transfer*, 41(24):4297 – 4313, 1998.
- [13] Shuichi Torii and Wen-Jei Yang. Thermal-fluid transport phenomena in strongly heated channel flows. *International Journal of Numerical Methods for Heat & Fluid Flow*, 10(8):802–823, 2000.
- [14] Dariusz P. Mikielwicz, A.Mohsen Shehata, J.Derek Jackson, and Donald M. McEligot. Temperature, velocity and mean turbulence structure in strongly heated internal gas flows: Comparison of numerical predictions with data. *International Journal of Heat and Mass Transfer*, 45(21):4333 – 4352, 2002.
- [15] Shuichi Torii and Wen-Jei Yang. Effect of heat flux ratio on two-dimensional horizontal channel flow. *Journal of Thermophysics and Heat Transfer*, 18(1):73–78, 2004.
- [16] Joong Hun Bae, Jung Yul Yoo, and Haecheon Choi. Direct numerical simulation of turbulent supercritical flows with heat transfer. *Physics of Fluids*, 17(10):105104, 2005.
- [17] S. Gordeev, V. Heinzl, and V. Slobodtchouk. Features of convective heat transfer in heated helium channel flow. *International Journal of Heat and Mass Transfer*, 48(16):3363 – 3380, 2005.
- [18] Joong Hun Bae, Jung Yul Yoo, Haecheon Choi, and Donald M. McEligot. Effects of large density variation on strongly heated internal air flows. *Physics of Fluids*, 18(7):075102, 2006.

- [19] Joong Hun Bae, Jung Yul Yoo, and Donald M. McEligot. Direct numerical simulation of heated CO₂ flows at supercritical pressure in a vertical annulus at Re=8900. *Physics of Fluids*, 20(5):055108, 2008.
- [20] S. He, W.S. Kim, and J.H. Bae. Assessment of performance of turbulence models in predicting supercritical pressure heat transfer in a vertical tube. *International Journal of Heat and Mass Transfer*, 51(19):4659 – 4675, 2008.
- [21] S. He, W.S. Kim, and J.D. Jackson. A computational study of convective heat transfer to carbon dioxide at a pressure just above the critical value. *Applied Thermal Engineering*, 28(13):1662 – 1675, 2008.
- [22] J.I. Lee, P. Hejzlar, P. Saha, P. Stahle, M.S. Kazimi, and D.M. McEligot. Deteriorated turbulent heat transfer (DTHT) of gas up-flow in a circular tube: Experimental data. *International Journal of Heat and Mass Transfer*, 51(13):3259 – 3266, 2008.
- [23] J.I. Lee, P. Hejzlar, P. Saha, M.S. Kazimi, and D.M. McEligot. Deteriorated turbulent heat transfer (DTHT) of gas up-flow in a circular tube: Heat transfer correlations. *International Journal of Heat and Mass Transfer*, 51(21):5318 – 5326, 2008.
- [24] Yuming Chen, Frederik Arbeiter, and Georg Schlindwein. A comparative study of turbulence models for conjugate heat transfer to gas flow in a heated mini-channel. *Numerical Heat Transfer, Part A: Application*, 61(1):38–60, 2012.
- [25] Biswadip Shome. Numerical study of turbulent flow in heated circular tube using transitional shear stress transport turbulence model. *International Journal of Thermal Sciences*, 79:90 – 102, 2014.
- [26] Francesco Zonta, Cristian Marchioli, and Alfredo Soldati. Modulation of turbulence in forced convection by temperature-dependent viscosity. *Journal of Fluid Mechanics*, 697:150–174, 2012.
- [27] Francesco Zonta, Miguel Onorato, and Alfredo Soldati. Turbulence and internal waves in stably-stratified channel flow with temperature-dependent fluid properties. *Journal of Fluid Mechanics*, 697:175–203, 2012.
- [28] Valentin Boutrouche, Erwin Franquet, Sylvain Serra, and Rémi Manceau. Influence of the turbulence model for channel flows with strong transverse temperature gradients. *International Journal of Heat and Fluid Flow*, 70:79–103, 2018.
- [29] Wen-Ping Wang and Richard H. Pletcher. On the large eddy simulation of a turbulent channel flow with significant heat transfer. *Physics of Fluids*, 8(12):3354–3366, 1996.
- [30] Bamdad Lessani and Miltiadis V. Papalexandris. Time-accurate calculation of variable density flows with strong temperature gradients and combustion. *Journal of Computational Physics*, 212:218–246, 2006.
- [31] Bamdad Lessani and Miltiadis V. Papalexandris. Numerical study of turbulent channel flow with strong temperature gradients. *International Journal of Numerical Methods for Heat & Fluid Flow*, 18(3/4):545–556, 2008.
- [32] Sylvain Serra, Adrien Toutant, and Françoise Bataille. Thermal large eddy simulation in a very simplified geometry of a solar receiver. *Heat Transfer Engineering*, 33(6):505–524, 2012.
- [33] J. Kim and P. Moin. Transport of passive scalars in a turbulent channel flow. In *Turbulent Shear Flows 6. Selected Papers from the 6th Int. Symp. Turb. Shear Flow, Toulouse, France, September 7-9, 1987*, Springer-Verlag, 1989.
- [34] N. Kasagi, Y. Tomita, and A. Kuroda. Direct numerical simulation of passive scalar field in a turbulent channel flow. *ASME J. Heat Transfer*, 114(3):598–606, 1992.

- [35] N. Kasagi and M. Nishimura. Direct Numerical Simulation of Combined Forced and Natural Turbulent Convection in a Vertical Plane Channel. *International Journal of Heat and Fluid Flow*, 18(1):88–99, 1997.
- [36] R. Boudjemadi, V. Maupu, D. Laurence, and P. Le Quéré. Budgets of turbulent stresses and fluxes in a vertical slot natural convection flow at Rayleigh $Ra = 10^5$ and $5.4 \cdot 10^5$. *International Journal of Heat and Fluid Flow*, 18(1):70–79, 1997.
- [37] Hiroshi Kawamura, Hiroyuki Abe, and Yuichi Matsuo. DNS of turbulent heat transfer in channel flow with respect to Reynolds and Prandtl number effects. *International Journal of Heat and Fluid Flow*, 20(3):196–207, 1999.
- [38] Makoto Kozuka, Yohji Seki, and Hiroshi Kawamura. DNS of turbulent heat transfer in a channel flow with a high spatial resolution. *International Journal of Heat and Fluid Flow*, 30(3):514 – 524, 2009. The Seventh International Symposium on Engineering Turbulence Modelling and Measurements, ETMM7.
- [39] T.A.M. Versteegh and F.T.M. Nieuwstadt. A direct numerical simulation of natural convection between two infinite vertical differentially heated walls scaling laws and wall functions. *International Journal of Heat and Mass Transfer*, 42(19):3673–3693, 1999.
- [40] P. Kiš and H. Herwig. The near wall physics and wall functions for turbulent natural convection. *International Journal of Heat and Mass Transfer*, 55(9-10):2625–2635, 2012.
- [41] Hirofumi Hattori, Shohei Yamada, Masahiro Tanaka, Tomoya Houra, and Yasutaka Nagano. DNS, LES and RANS of turbulent heat transfer in boundary layer with suddenly changing wall thermal conditions. *International Journal of Heat and Fluid Flow*, 41(Supplement C):34 – 44, 2013. ETMM9.
- [42] Cédric Flageul, Sofiane Benhamadouche, Éric Lamballais, and Dominique Laurence. DNS of turbulent channel flow with conjugate heat transfer: Effect of thermal boundary conditions on the second moments and budgets. *International Journal of Heat and Fluid Flow*, 55(Supplement C):34 – 44, 2015. Special Issue devoted to the 10th Int. Symposium on Engineering Turbulence Modelling and Measurements (ETMM10) held in Marbella, Spain on September 17-19, 2014.
- [43] Sergio Pirozzoli, Matteo Bernardini, Roberto Verzicco, and Paolo Orlandi. Mixed convection in turbulent channels with unstable stratification. *Journal of Fluid Mechanics*, 821:482–516, 2017.
- [44] Franck Nicoud and Thierry Poinsot. DNS of a channel flow with variable properties. In *TSFP DIGITAL LIBRARY ONLINE*. Begel House Inc., 1999.
- [45] B. Debusschere and C.J. Rutland. Turbulent scalar transport mechanisms in plane channel and Couette flows. *International Journal of Heat and Mass Transfer*, 47(8):1771–1781, 2004.
- [46] Frédéric Auléry, Adrien Toutant, Françoise Bataille, and Ye Zhou. Energy transfer process of anisothermal wall-bounded flows. *Physics Letters A*, 379(24):1520–1526, 2015.
- [47] Ashish Patel, Jurriaan W. R. Peeters, Bendiks J. Boersma, and Rene Pecnik. Semi-local scaling and turbulence modulation in variable property turbulent channel flows. *Physics of Fluids*, 27(9):095101, 2015.
- [48] Ashish Patel, Bendiks J. Boersma, and Rene Pecnik. The influence of near-wall density and viscosity gradients on turbulence in channel flows. *Journal of Fluid Mechanics*, 809:793–820, 2016.
- [49] Sylvain Serra, Adrien Toutant, Françoise Bataille, and Ye Zhou. High-temperature gradient effect on a turbulent channel flow using thermal large-eddy simulation in physical and spectral spaces. *Journal of Turbulence*, 13:1–25, 2012.
- [50] Sylvain Serra, Adrien Toutant, Françoise Bataille, and Ye Zhou. Turbulent kinetic energy spectrum in very anisothermal flows. *Physics Letters A*, 376:3177–3184, 2012.

- [51] Syed Mohd Yahya, Syed Fahad Anwer, and Sanjeev Sanghi. Turbulent forced convective flow in an anisothermal channel. *International Journal of Thermal Sciences*, 88:84–95, 2015.
- [52] A. Pucciarelli and W. Ambrosini. Improvements in the prediction of heat transfer to supercritical pressure fluids by the use of algebraic heat flux models. *Annals of Nuclear Energy*, 99(Supplement C):58 – 67, 2017.
- [53] Y. Nagano and C. Kim. A two-equation model for heat transport in wall turbulent shear flows. *ASME J. Heat Transfer*, 110(3):583–589, 1988.
- [54] W. Sutherland. The viscosity of gases and molecular force. *Philosophical Magazine Series 5*, 36(223):507–531, 1893.
- [55] C. Flageul, I. Tiselj, S. Benhamadouche, and M. Ferrand. A correlation for the discontinuity of the temperature variance dissipation rate at the fluid-solid interface in turbulent channel flows. *Flow, Turb. Combust.*, 103(1):175–201, 2019.
- [56] P. Sagaut. *Large eddy simulation for incompressible flows*. Springer, third edition, 2006.
- [57] Florian R. Menter. Zonal two equation $k - \omega$ turbulence models for aerodynamic flows. In *AIAA Fluid Dynamics Conference*, volume 93, page 2906, 1993.
- [58] Florian R. Menter. Two-equation eddy-viscosity turbulence models for engineering applications. *AIAA Journal*, 32(8):1598–1605, 1994.
- [59] F. Billard and D. Laurence. A robust $k-\varepsilon/k$ elliptic blending turbulence model applied to near-wall, separated and buoyant flows. *International Journal of Heat and Fluid Flow*, 33(1):45–58, 2012.
- [60] Rémi Manceau and Kemal Hanjalić. Elliptic blending model: A new near-wall Reynolds-stress turbulence closure. *Physics of Fluids (1994-present)*, 14(2):744–754, 2002.
- [61] R. Manceau. Recent progress in the development of the elliptic blending Reynolds-stress model. *International Journal of Heat and Fluid Flow*, 51:195–220, 2015.
- [62] John Kim, Parviz Moin, and Robert Moser. Turbulence statistics in fully developed channel flow at low Reynolds number. *Journal of Fluid Mechanics*, 177:133–166, 1987.
- [63] Guillaume Brilliant, Sabine Husson, and Françoise Bataille. Subgrid-scale diffusivity: Wall behavior and dynamic methods. *Journal of Applied Mechanics*, 73(3):360–367, 2006.
- [64] Sabine Husson. *Simulations des grandes échelles pour les écoulements turbulents anisothermes*. PhD thesis, Institut National des Sciences Appliquées de Lyon, 2007.
- [65] A. Châtelain, F. Ducros, and O. Métais. LES of turbulent heat transfer: proper convection numerical schemes for temperature transport. *International Journal for Numerical Methods in Fluids*, 44(9):1017–1044, 2004.
- [66] Adrien Toutant and Françoise Bataille. Turbulence statistics in a fully developed channel flow submitted to a high temperature gradient. *International Journal of Thermal Sciences*, 74:104 – 118, 2013.
- [67] Francesco Zonta and Alfredo Soldati. Effect of temperature dependent fluid properties on heat transfer in turbulent mixed convection. *ASME J. Heat Transfer*, 136(2):022501–022501–12, 2014.
- [68] F.R. Menter, M. Kuntz, and R. Langtry. Ten years of industrial experience with the SST turbulence model. In *Proc. 4th Int. Symp. Turbulence, Heat and Mass Transfer, Antalya, Turkey*, 2003.

- [69] Frédéric Archambeau, Namane Méchitoua, and Marc Sakiz. Code saturne: a finite volume code for the computation of turbulent incompressible flows, industrial applications. *International Journal on Finite Volumes*, 1(1):1–62, 2004.
- [70] Mohammadreza Sedighi, Ricardo Vasquez Padilla, Robert A. Taylor, Maree Lake, Iman Izadgoshasb, and Andrew Rose. High-temperature, point-focus, pressurised gas-phase solar receivers: A comprehensive review. *Energy Conversion and Management*, 185:678 – 717, 2019.
- [71] M.I. Roldán, A. Avila-Marin, M. Alvarez-Lara, and J. Fernandez-Reche. Experimental and numerical characterization of ceramic and metallic absorbers under lab-scale conditions. *Energy Procedia*, 69:523 – 531, 2015. International Conference on Concentrating Solar Power and Chemical Energy Systems, SolarPACES 2014.
- [72] A.L. Avila-Marin, M. Alvarez-Lara, and J. Fernandez-Reche. Experimental results of gradual porosity wire mesh absorber for volumetric receivers. *Energy Procedia*, 49:275 – 283, 2014. Proceedings of the SolarPACES 2013 International Conference.
- [73] D. Hirsch, P. v. Zedtwitz, T. Osinga, J. Kinamore, and A. Steinfeld. A New 75 kW High-Flux Solar Simulator for High-Temperature Thermal and Thermochemical Research. *Journal of Solar Energy Engineering*, 125(1):117–120, 01 2003.
- [74] Jin Lee, Seo Yoon Jung, Hyung Jin Sung, and Tamer A. Zaki. Turbulent thermal boundary layers with temperature-dependent viscosity. *International Journal of Heat and Fluid Flow*, 49(Supplement C):43 – 52, 2014. 8th Symposium on Turbulence & Shear Flow Phenomena (TSFP8).
- [75] Takahiro Tsukahara. DNS of turbulent channel flow at very low reynolds numbers. *ArXiv e-prints*, 06 2014.
- [76] A. Fortin, M. Jardak, J.J. Gervais, and R. Pierre. Old and new results on the two-dimensional Poiseuille flow. *Journal of Computational Physics*, 115(2):455 – 469, 1994.
- [77] Franck Nicoud. Numerical study of a channel flow with variable properties. *CTR Annual Research Briefs*, pages 289–309, 1998.
- [78] Jin Lee, Seo Yoon Jung, Hyung Jin Sung, and Tamer A. Zaki. Effect of wall heating on turbulent boundary layers with temperature-dependent viscosity. *Journal of Fluid Mechanics*, 726:196–225, 2013.
- [79] Frederic Aulery, Dorian Dupuy, Adrien Toutant, Françoise Bataille, and Ye Zhou. Spectral analysis of turbulence in anisothermal channel flows. *Computers & Fluids*, 151:115–131, 2017.
- [80] Hiroyuki Abe, Hiroshi Kawamura, and Yuichi Matsuo. Surface heat-flux fluctuations in a turbulent channel flow up to $Re_\tau=1020$ with $Pr=0.025$ and 0.71 . *International Journal of Heat and Fluid Flow*, 25(3):404 – 419, 2004. Turbulence and Shear Flow Phenomena (TSFP-3).
- [81] Alexandre Chatelain, Frédéric Ducros, and Olivier Métais. Large eddy simulation of conjugate heat-transfer using thermal wall-functions. In Rainer Friedrich, Bernard J. Geurts, and Olivier Métais, editors, *Direct and Large-Eddy Simulation V*, pages 307–314, Dordrecht, 2004. Springer Netherlands.
- [82] Dorian Dupuy, Adrien Toutant, and Françoise Bataille. Turbulence kinetic energy exchanges in flows with highly variable fluid properties. *Journal of Fluid Mechanics*, 834:5–54, 2018.
- [83] Jin Lee, Jae Hwa Lee, Jung-Il Choi, and Hyung Jin Sung. Spatial organization of large- and very-large-scale motions in a turbulent channel flow. *Journal of Fluid Mechanics*, 749:818–840, 2014.
- [84] B. Ničeno and M. Sharabi. Large eddy simulation of turbulent heat transfer at supercritical pressures. *Nuclear Engineering and Design*, 261(Supplement C):44 – 55, 2013.

-
- [85] Franck Nicoud. Conservative high-order finite-difference schemes for low-Mach number flows. *Journal of Computational Physics*, 158:71–97, 2000.
- [86] P. Orlandi, D. Sassun, and S. Leonardi. DNS of conjugate heat transfer in presence of rough surfaces. *International Journal of Heat and Mass Transfer*, 100(Supplement C):250 – 266, 2016.
- [87] Dimitrios V. Papavassiliou and Thomas J. Hanratty. Transport of a passive scalar in a turbulent channel flow. *International Journal of Heat and Mass Transfer*, 40(6):1303 – 1311, 1997.
- [88] H. C. Perkins and P. Worsoe-Schmidt. Turbulent heat and momentum transfer for gases in a circular tube at wall to bulk temperature ratios to seven. *International Journal of Heat and Mass Transfer*, 8(7):1011 – 1031, 1965.
- [89] S. Saha, J.C. Klewicki, A.S.H. Ooi, and H.M. Blackburn. Comparison of thermal scaling properties between turbulent pipe and channel flows via DNS. *International Journal of Thermal Sciences*, 89(Supplement C):43 – 57, 2015.
- [90] M. Sanchez, F. Aulery, Toutant A., and Bataille F. Large eddy simulations of thermal boundary layer spatial development in a turbulent channel flow. *ASME J. Fluids Eng.*, 136(6):060906–060906–12, 2014.
- [91] A. Scagliarini, H. Einarsson, Á. Gylfason, and F. Toschi. Law of the wall in an unstably stratified turbulent channel flow. *Journal of Fluid Mechanics*, 781, 2015.
- [92] Iztok Tiselj and Leon Cizelj. DNS of turbulent channel flow with conjugate heat transfer at Prandtl number 0.01. *Nuclear Engineering and Design*, 253(Supplement C):153 – 160, 2012.
- [93] Iztok Tiselj, Jure Oder, and Leon Cizelj. Double-sided cooling of heated slab: Conjugate heat transfer DNS. *International Journal of Heat and Mass Transfer*, 66:781 – 790, 2013.
- [94] Iztok Tiselj. Tracking of large-scale structures in turbulent channel with direct numerical simulation of low Prandtl number passive scalar. *Physics of Fluids*, 26(12):125111, 2014.

A Overview of some available studies dealing with thermal effects on turbulent flows

In the main document, Table 1 presents a summary of the papers on laminarization of turbulent flows. Since this topic belongs to a larger one, where impacts of heat transfer are considered, Table 5 provides a list of studies on the influence of thermal effects on the behavior of turbulent flows.

Table 5 – Studies on heat effects on turbulent flows

Ref.	Type	Flow			Geometry				Orient.		Thermal cond.			Modelling	
		forced	natural	mixed	plate	tube	annulus	channel	hor.	ver.	imp. temp.	imp. flux	heat source	passive scal.	dep. param.
80	DNS	✓						✓			✓			✓	
46	DNS	✓						✓			✓				✓
79	DNS / LES	✓						✓			✓				✓
16	DNS	✓		✓		✓			✓			✓			✓
18	DNS	✓		✓		✓			✓			✓			✓
19	DNS	✓		✓			✓		✓			✓		✓	✓
6	Exp.	✓				✓			✓			✓			n.a.
28	RANS	✓						✓			✓				✓
81	LES	✓						✓				✓		✓	
24	RANS	✓						✓				✓			✓
7	Exp.	✓				✓			✓			✓			n.a.
45	DNS	✓						✓			✓			✓	
82	DNS	✓						✓			✓				✓
17	RANS	✓						✓				✓			✓
41	DNS / LES / RANS	✓			✓			✓			✓	✓		✓	
20	DNS	✓		✓		✓			✓			✓			✓
21	RANS	✓		✓		✓			✓			✓			✓
34	DNS	✓						✓				✓		✓	
35	DNS		✓	✓				✓		✓			✓	✓	
37	DNS	✓						✓				✓		✓	
38	DNS	✓						✓				✓		✓	
22	Exp.			✓		✓			✓			✓			n.a.
23	Exp.			✓		✓			✓			✓			n.a.
78	DNS	✓			✓				✓			✓		✓	
74	DNS	✓			✓				✓			✓		✓	
83	DNS	✓			✓				✓			✓		✓	
30	LES	✓						✓				✓			✓
31	LES	✓						✓				✓			✓
14	RANS	✓				✓			✓				✓		✓
12	Exp.	✓				✓			✓			✓			n.a.
84	LES	✓		✓		✓			✓			✓			✓
77	DNS	✓						✓				✓			✓
44	DNS	✓						✓				✓			✓

.....

Table 5 – continued...

Ref.	Type	forced	natural	mixed	plate	tube	annulus	channel	hor.	ver.	imp. temp.	imp. flux	heat source	passive scal.	dep. param.
85	DNS	✓						✓	✓		✓				✓
86	DNS	✓						✓	✓		✓			✓	
87	DNS	✓						✓	✓		✓			✓	
47	DNS	✓						✓	✓				✓		✓
48	DNS	✓						✓	✓				✓		✓
88	Exp.	✓				✓			✓			✓			n.a.
8	Exp.	✓		✓				✓		✓		✓			n.a.
43	DNS			✓				✓		✓	✓			✓	
52	RANS		✓					✓	✓			✓		✓	
89	DNS	✓				✓		✓	✓		✓			✓	
90	LES	✓						✓	✓		✓				✓
91	DNS	✓		✓				✓	✓		✓			✓	
32	LES	✓						✓	✓		✓				✓
49	LES	✓						✓	✓		✓				✓
50	LES	✓						✓	✓		✓				✓
25	RANS	✓		✓		✓		✓		✓		✓			✓
92	DNS	✓						✓	✓				✓		✓
93	DNS	✓						✓	✓				✓		✓
94	DNS	✓						✓	✓				✓		✓
9	RANS	✓				✓			✓			✓		✓	
10	RANS	✓					✓		✓			✓		✓	
11	RANS	✓				✓			✓			✓		✓	
13	RANS	✓						✓	✓			✓		✓	
15	RANS	✓				✓			✓			✓		✓	
66	DNS	✓						✓	✓		✓				✓
29	LES	✓						✓	✓		✓				✓
51	LES	✓						✓	✓		✓				✓
26	DNS	✓						✓	✓		✓			✓	
27	DNS			✓				✓		✓				✓	
67	DNS	✓						✓	✓		✓			✓	

B RANS models

B.1 $k - \omega - \text{SST}$ equations

$$\rho \frac{dk}{dt} = \rho \mathcal{P}_k - \beta^* \rho \omega k + \frac{\partial}{\partial x_i} \left[\left(\mu + \frac{\mu_t}{\sigma_k} \right) \frac{\partial k}{\partial x_i} \right] \quad (\text{B.20a})$$

$$\rho \frac{d\omega}{dt} = \frac{\gamma}{\nu_t} \rho \mathcal{P}_k - \beta \rho \omega^2 + \frac{\partial}{\partial x_i} \left[\left(\mu + \frac{\mu_t}{\sigma_\omega} \right) \frac{\partial \omega}{\partial x_i} \right] + 2(1 - F_1) \rho \sigma_\omega \frac{1}{\omega} \frac{\partial k}{\partial x_i} \frac{\partial \omega}{\partial x_i} \quad (\text{B.20b})$$

With :

$$\nu_t = \frac{a_1 k}{\max(a_1 \omega, SF_2)} \quad (\text{B.21a})$$

$$\mathcal{P}_k = \min \left(-\tau_{ij} \frac{\partial \bar{U}_i}{\partial x_j}, 10 \beta^* k \omega \right) \quad (\text{B.21b})$$

$$F_1 = \tanh \left[\left[\min \left[\max \left(\frac{\sqrt{k}}{\beta^* \omega y}, \frac{500 \nu}{y^2 \omega} \right), \frac{4 \rho \sigma_{\omega_2} k}{\text{CD}_{k\omega} y^2} \right] \right]^4 \right] \quad (\text{B.21c})$$

$$F_2 = \tanh \left[\left[\max \left(\frac{2\sqrt{k}}{\beta^* \omega y}, \frac{500 \nu}{y^2 \omega} \right) \right]^2 \right] \quad (\text{B.21d})$$

$$\text{CD}_{k\omega} = \max \left(2 \rho \sigma_{\omega_2} \frac{1}{\omega} \frac{\partial k}{\partial x_i} \frac{\partial \omega}{\partial x_i}, 10^{-10} \right) \quad (\text{B.21e})$$

The constant ϕ are computed from the constants ϕ_1 and ϕ_2 :

Table 6 – $k - \omega - \text{SST}$ constants

	σ_k	σ_ω	β	γ
ϕ_1	1.1765	2.0	0.075	0.54
ϕ_2	1.0	1.1682	0.0828	0.42

B.2 $k - \varepsilon - \overline{v^2}/k$ equations

$$\rho \frac{dk}{dt} = \rho \mathcal{P} - \rho \varepsilon + \frac{\partial}{\partial x_i} \left[\left(\frac{\mu}{2} + \frac{\mu_t}{\sigma_k} \right) \frac{\partial k}{\partial x_i} \right] - C_{\varepsilon 3} (1 - \alpha)^3 \rho \frac{k}{\varepsilon} 2 \nu \nu_t (\partial_k \partial_j \bar{U}_i) (\partial_k \partial_j \bar{U}_i), \quad (\text{B.22a})$$

$$\rho \frac{d\varepsilon}{dt} = \frac{C_{\varepsilon 1} \rho \mathcal{P} - C_{\varepsilon 2}^* \rho \varepsilon}{\mathbb{T}} + \frac{\partial}{\partial x_i} \left[\left(\frac{\mu}{2} + \frac{\mu_t}{\sigma_k} \right) \frac{\partial \varepsilon}{\partial x_i} \right], \quad (\text{B.22b})$$

$$\frac{d\varphi}{dt} = (1 - \alpha^3) f_w + \alpha^3 f_h - \mathcal{P} \frac{\varphi}{k} + \frac{2}{k} \frac{\nu_t}{\sigma_k} \frac{\partial \varphi}{\partial x_i} \frac{\partial k}{\partial x_i} + \frac{\partial}{\partial x_i} \left[\left(\frac{\nu}{2} + \frac{\nu_t}{\sigma_\varphi} \right) \frac{\partial \varphi}{\partial x_i} \right], \quad (\text{B.22c})$$

$$\alpha - \mathcal{L}^2 \nabla^2 \alpha = 1. \quad (\text{B.22d})$$

With:

$$\nu_t = C_\mu \varphi k \min(\mathbb{T}, \mathbb{T}_{lim}) \quad (\text{B.23a})$$

$$\mathbb{T} = \sqrt{\frac{k^2}{\varepsilon^2} + C_T^2 \frac{\nu}{\varepsilon}} \quad (\text{B.23b})$$

$$\mathbb{T}_{lim} = \frac{0.6}{\sqrt{6} C_\mu \varphi \sqrt{\underline{\underline{\mathcal{S}}:\underline{\underline{\mathcal{S}}}}} } \quad (\text{B.23c})$$

And;

$$f_w = -\frac{\varepsilon \varphi}{2k} \quad (\text{B.24a})$$

$$f_h = -\frac{1}{\mathbb{T}} \left(C_1 - 1 + C_2 \frac{\mathcal{P}}{\varepsilon} \right) \left(\varphi - \frac{2}{3} \right) \quad (\text{B.24b})$$

$$C_{\varepsilon 2}^* = C_{\varepsilon 2} + \alpha^3 (C_{\varepsilon 4} - C_{\varepsilon 2}) \tanh \left(\left| \frac{\frac{\partial}{\partial x_i} \left(\frac{\nu_t}{\sigma_k} \frac{\partial k}{\partial x_i} \right)}{\varepsilon} \right|^{3/2} \right) \quad (\text{B.24c})$$

$$\mathcal{L} = \sqrt{C_L^2 \left(\frac{k^3}{\varepsilon^2} + C_\eta^2 \frac{\nu^{3/2}}{\varepsilon^{1/2}} \right)} \quad (\text{B.24d})$$

And:

Table 7 – $k - \varepsilon - \overline{v^2}/k$ constants

$C_{\varepsilon 1}$	$C_{\varepsilon 2}$	$C_{\varepsilon 3}$	$C_{\varepsilon 4}$	σ_k	σ_ε	C_μ	C_T	C_L	C_η	C_1	C_2	σ_φ
1.44	1.83	2.3	0.4	1	1.5	0.22	4	0.164	75	1.7	0.9	1

B.3 EB-RSM equations

$$\frac{d\rho \overline{U'_i U'_j}}{dt} = \rho \mathcal{P}_{ij} + \rho \phi_{ij} - \rho \varepsilon_{ij} + D_{ij}^\mu + D_{ij}^T, \quad (\text{B.25a})$$

$$\frac{d\rho \varepsilon}{dt} = \frac{C'_{\varepsilon 1} \rho \mathcal{P} - C_{\varepsilon 2} \rho \varepsilon}{\mathbb{T}} + \frac{\partial}{\partial x_k} \left(\frac{C_\mu}{\sigma_\varepsilon} \rho \tau_{kl} \mathbb{T} \frac{\partial \varepsilon}{\partial x_l} \right) + \frac{\partial}{\partial x_k} \left(\mu \frac{\partial \varepsilon}{\partial x_k} \right), \quad (\text{B.25b})$$

$$\alpha - \mathcal{L}^2 \nabla^2 \alpha = 1. \quad (\text{B.25c})$$

with:

$$\phi_{ij} = (1 - \alpha^3)\phi_{ij}^w + \alpha^3\phi_{ij}^h \quad (\text{B.26a})$$

$$\varepsilon_{ij} = (1 - \alpha^3)\varepsilon_{ij}^w + \alpha^3\varepsilon_{ij}^h \quad (\text{B.26b})$$

$$\mathcal{L} = C_L \max\left(\frac{k^{3/2}}{\varepsilon}; C_\eta \frac{\nu^{3/4}}{\varepsilon^{1/4}}\right) \quad (\text{B.26c})$$

$$\mathbb{T} = \max\left(\frac{k}{\varepsilon}; C_T \sqrt{\frac{\nu}{\varepsilon}}\right) \quad (\text{B.26d})$$

$$C'_{\varepsilon 1} = C_{\varepsilon 1} \left(1 + A_1(1 - \alpha^3)\frac{\mathcal{P}}{\varepsilon}\right) \quad (\text{B.26e})$$

$$\mathbf{n} = \frac{\nabla\alpha}{\|\nabla\alpha\|} \quad (\text{B.26f})$$

$$\phi_{ij}^h = -(C_1\varepsilon + C'_2\mathcal{P})a_{ij} + \left(C_3 - C'_3(a_{kl}a_{kl})^{0.5}\right)kS_{ij} + C_4k\left(a_{ik}S_{jk} + a_{jk}S_{ik} - \frac{2}{3}a_{kl}S_{kl}\delta_{ij}\right) \quad (\text{B.26g})$$

$$+ C_5(a_{ik}\Omega_{jk} + a_{jk}\Omega_{ik}) \quad (\text{B.26h})$$

$$\phi_{ij}^w = -5\frac{\varepsilon}{k}\left[\tau_{ik}n_jn_k + \tau_{jk}n_in_k - \frac{1}{2}\tau_{kl}n_kn_l(n_in_j + \delta_{ij})\right] \quad (\text{B.26i})$$

$$\tau_{ij} = \overline{U'_iU'_j} \quad (\text{B.26j})$$

$$\varepsilon_{ij}^w = \frac{\overline{U'_iU'_j}}{k}\varepsilon \quad (\text{B.26k})$$

$$\varepsilon_{ij}^h = \frac{2}{3}\varepsilon\delta_{ij} \quad (\text{B.26l})$$

$$a_{ij} = \frac{\overline{U'_iU'_j}}{k} - \frac{2}{3}\delta_{ij} \quad (\text{B.26m})$$

$$\Omega_{ij} = \frac{1}{2}\left(\frac{\partial\overline{U}_i}{\partial x_j} - \frac{\partial\overline{U}_j}{\partial x_i}\right) \quad (\text{B.26n})$$

$$\mathcal{P}_{ij} = -\overline{U'_iU'_k}\frac{\partial\overline{U}_j}{\partial x_k} - \overline{U'_jU'_k}\frac{\partial\overline{U}_i}{\partial x_k} \quad (\text{B.26o})$$

$$D_{ij}^T = \frac{\partial}{\partial x_l}\left(\rho\frac{C_\mu}{\sigma_k}\overline{U'_lU'_m}\mathbb{T}\frac{\partial\overline{U'_iU'_j}}{\partial x_m}\right) \quad (\text{B.26p})$$

And:

Table 8 – EB-RSM constants

C_1	C'_2	C_3	C'_3	C_4	C_5	C_L	C_η	C_T	$C_{\varepsilon 1}$	A_1	$C_{\varepsilon 2}$	σ_ε
1.7	0.9	0.8	0.65	0.625	0.2	0.122	80	6	1.44	0.1	1.83	1.15